



HAL
open science

Search for technicolor with DELPHI

J. Abdallah, P. Abreu, W. Adam, P. Adzic, T. Albrecht, T. Alderweireld, R. Alemany-Fernandez, P P. Allport, S. Almeded, T. Almendinger, et al.

► **To cite this version:**

J. Abdallah, P. Abreu, W. Adam, P. Adzic, T. Albrecht, et al.. Search for technicolor with DELPHI. European Physical Journal C: Particles and Fields, 2001, 22, pp.17-29. <10.1007/s100520100782>. <in2p3-00011007>

HAL Id: in2p3-00011007

<https://in2p3.hal.science/in2p3-00011007v1>

Submitted on 5 Dec 2001

HAL is a multi-disciplinary open access archive for the deposit and dissemination of scientific research documents, whether they are published or not. The documents may come from teaching and research institutions in France or abroad, or from public or private research centers.

L'archive ouverte pluridisciplinaire HAL, est destinée au dépôt et à la diffusion de documents scientifiques de niveau recherche, publiés ou non, émanant des établissements d'enseignement et de recherche français ou étrangers, des laboratoires publics ou privés.



HAL Authorization

Search for Technicolor with DELPHI

DELPHI Collaboration

Abstract

Technicolor represents a viable alternative to the Higgs mechanism for generating gauge boson masses. Searches for technicolor particles ρ_T and π_T have been performed in the data collected by the DELPHI experiment at LEP at centre-of-mass energies between 192 and 208 GeV corresponding to an integrated luminosity of 452 pb^{-1} . Good agreement is observed with the SM expectation in all channels studied. This is translated into an excluded region in the (M_{π_T}, M_{ρ_T}) plane. The ρ_T production is excluded for all $90 < M_{\rho_T} < 206.7 \text{ GeV}/c^2$. Assuming a point-like interaction of the π_T with gauge bosons, an absolute lower limit on the charged π_T mass at 95% CL is set at $79.8 \text{ GeV}/c^2$, independently of other parameters of the technicolor model.

(Accepted by Eur.Phys.J.C)

J.Abdallah²³, P.Abreu²¹, W.Adam⁴⁸, P.Adzic¹¹, T.Albrecht¹⁶, T.Alderweireld², R.Aleman-Fernandez⁸, P.P.Allport²²,
 S.Almehed²⁴, T.Almendinger¹⁶, U.Amaldi²⁷, N.Amapane⁴³, S.Amato⁴⁵, E.Anashkin³⁴, A.Andrezza²⁶, S.Andringa²¹,
 N.Anjos²¹, P.Antilogus²⁵, W-D.Apel¹⁶, Y.Arnoud¹³, S.Ask²⁴, B.Asman⁴², J.E.Augustin²³, A.Augustinus⁸, P.Baillon⁸,
 A.Ballestrero⁴³, P.Bambade¹⁹, R.Barbier²⁵, D.Bardin¹⁵, G.Barker¹⁶, A.Baroncelli³⁷, M.Baubillier²³, K-H.Becks⁵⁰,
 M.Begalli⁶, A.Behrmann⁵⁰, T.Bellunato⁸, N.Benekos³⁰, A.Benvenuti⁵, C.Berat¹³, L.Berntzon⁴², D.Bertrand²,
 M.Besancon³⁸, N.Besson³⁸, D.Bloch⁹, M.Blom²⁹, I.Boiko¹⁵, M.Bonesini²⁷, M.Boonekamp³⁸, P.S.L.Booth²²,
 G.Borisov^{8,20}, O.Botner⁴⁶, B.Bouquet¹⁹, T.J.V.Bowcock²², M.Bracko⁴¹, R.Brenner⁴⁶, E.Brodet³³, J.Brodzicka¹⁷,
 P.Bruckman¹⁷, J.M.Brunet⁷, L.Bugge³¹, P.Buschmann⁵⁰, M.Calvi²⁷, T.Camporesi⁸, V.Canale³⁶, F.Carena⁸,
 C.Carimalo²³, N.Castro²¹, F.Cavallo⁵, M.Chapkin⁴⁰, Ph.Charpentier⁸, P.Checchia³⁴, R.Chierici⁸, P.Chliapnikov⁴⁰,
 S.U.Chung⁸, K.Cieslik¹⁷, P.Collins⁸, R.Contri¹², G.Cosme¹⁹, F.Cossutti⁴⁴, M.J.Costa⁴⁷, B.Crawley¹, D.Crennell³⁵,
 J.Cuevas³², J.D'Hondt², J.Dalmau⁴², T.da Silva⁴⁵, W.Da Silva²³, G.Della Ricca⁴⁴, A.De Angelis⁴⁴, W.De Boer¹⁶,
 C.De Clercq², B.De Lotto⁴⁴, N.De Maria⁴³, A.De Min³⁴, L.de Paula⁴⁵, L.Di Ciaccio³⁶, A.Di Simone³⁷, K.Doroba⁴⁹,
 J.Drees⁵⁰, M.Dris³⁰, G.Eigen⁴, T.Ekelof⁴⁶, M.Ellert⁴⁶, M.Elsing⁸, M.C.Espirito Santo⁸, G.Fanourakis¹¹,
 D.Fassouliotis¹¹, M.Feindt¹⁶, J.Fernandez³⁹, A.Ferrer⁴⁷, F.Ferro¹², U.Flagmeyer⁵⁰, H.Foeth⁸, E.Fokitis³⁰,
 F.Fulda-Quenzer¹⁹, J.Fuster⁴⁷, M.Gandelman⁴⁵, C.Garcia⁴⁷, Ph.Gavillet⁸, E.Gazis³⁰, D.Gele⁹, T.Geralis¹¹,
 R.Gokieli^{8,49}, B.Golob⁴¹, G.Gomez-Ceballos³⁹, P.Goncalves²¹, R.Gonzalez Caballero³⁹, E.Graziani³⁷, G.Grosdidier¹⁹,
 K.Grzelak⁴⁹, J.Guy³⁵, C.Haag¹⁶, F.Hahn⁸, S.Hahn⁵⁰, A.Hallgren⁴⁶, K.Hamacher⁵⁰, K.Hamilton³³, J.Hansen³¹,
 S.Haug³¹, F.Hauler¹⁶, V.Hedberg²⁴, M.Hennecke¹⁶, H.Herr⁸, S-O.Holmgren⁴², P.J.Holt³³, M.A.Houlden²²,
 K.Hultqvist⁴², O.Iouchtchenko⁴⁰, J.N.Jackson²², P.Jalocha¹⁷, Ch.Jarlskog²⁴, G.Jarlskog²⁴, P.Jarry³⁸, D.Jeans³³,
 E.K.Johansson⁴², P.D.Johansson⁴², P.Jonsson²⁵, C.Joram⁸, L.Jungermann¹⁶, F.Kapusta²³, S.Katsanevas²⁵,
 E.Katsoufis³⁰, R.Keranen¹⁶, G.Kernel⁴¹, B.P.Kersevan^{8,41}, A.Kiiskinen¹⁴, B.T.King²², N.J.Kjaer⁸, P.Kluit²⁹,
 P.Kokkinias¹¹, C.Kourkoumelis³, O.Kouznetsov¹⁵, Z.Krumstein¹⁵, M.Kucharczyk¹⁷, J.Kurowska⁴⁹, J.Lamsa¹,
 G.Leder⁴⁸, F.Ledroit¹³, L.Leinonen⁴², R.Leitner²⁸, J.Lemone², G.Lenzen⁵⁰, V.Lepeltier¹⁹, T.Lesiak¹⁷, W.Liebig⁵⁰,
 D.Liko^{8,48}, A.Lipniacka⁴², J.H.Lopes⁴⁵, J.M.Lopez³², R.Lopez-Fernandez¹³, D.Loukas¹¹, P.Lutz³⁸, L.Lyons³³,
 J.MacNaughton⁴⁸, A.Malek⁵⁰, S.Maltezos³⁰, F.Mandl⁴⁸, J.Marco³⁹, R.Marco³⁹, B.Marechal⁴⁵, M.Margoni³⁴,
 J-C.Marin⁸, C.Mariotti⁸, A.Markou¹¹, C.Martinez-Rivero³⁹, J.Masik²⁸, N.Mastroiannopoulos¹¹, F.Matorras³⁹,
 C.Matteuzzi²⁷, F.Mazzucato³⁴, M.Mazzucato³⁴, R.Mc Nulty²², C.Meroni²⁶, T.Meyer¹, E.Migliore⁴³, W.Mitaroff⁴⁸,
 U.Mjoernmark²⁴, T.Moa⁴², M.Moch¹⁶, K.Moenig^{8,10}, R.Monge¹², J.Montenegro²⁹, D.Moraes⁴⁵, S.Moreno²¹,
 P.Morettini¹², U.Mueller⁵⁰, K.Muenich⁵⁰, M.Mulders²⁹, L.Mundim⁶, W.Murray³⁵, B.Muryn¹⁸, G.Myatt³³,
 T.Myklebust³¹, M.Nassiakou¹¹, F.Navarria⁵, K.Nawrocki⁴⁹, S.Nemecek²⁸, R.Nicolaidou³⁸, P.Niezurawski⁴⁹,
 M.Nikolenko^{15,9}, A.Nygren²⁴, A.Oblakowska-Mucha¹⁸, V.Obratsov⁴⁰, A.Olshevski¹⁵, A.Onofre²¹, R.Orava¹⁴,
 K.Osterberg⁸, A.Ouraou³⁸, A.Oyanguren⁴⁷, M.Paganoni²⁷, S.Paiano⁵, J.P.Palacios²², H.Palka¹⁷, Th.D.Papadopoulou³⁰,
 L.Pape⁸, C.Parkes²², F.Parodi¹², U.Parzefall²², A.Passerì³⁷, O.Passon⁵⁰, L.Peralta²¹, V.Perepelitsa⁴⁷, A.Perrotta⁵,
 A.Petrolini¹², J.Piedra³⁹, L.Pieri³⁷, F.Pierre³⁸, M.Pimenta²¹, E.Piotto⁸, T.Podobnik⁴¹, M.E.Pol⁶, G.Polok¹⁷,
 P.Poropat⁴⁴, V.Pozdniakov¹⁵, P.Privitera³⁶, N.Pukhaeva^{2,15}, A.Pullia²⁶, J.Rames²⁸, L.Ramler¹⁶, A.Read³¹,
 P.Rebecchi⁸, J.Rehn¹⁶, D.Reid²⁹, R.Reinhardt⁵⁰, P.Renton³³, D.Riabtchikov⁴⁰, F.Richard¹⁹, J.Ridky²⁸, I.Ripp-Baudot⁹,
 A.Romero⁴³, P.Ronchese³⁴, E.Rosenberg¹, P.Roudeau¹⁹, T.Rovelli⁵, V.Ruhmann-Kleider³⁸, A.Sadovsky¹⁵, L.Salmi¹⁴,
 J.Salt⁴⁷, A.Savoy-Navarro²³, C.Schwanda⁴⁸, B.Schwering⁵⁰, U.Schwickerath⁸, A.Segar³³, R.Sekulin³⁵, M.Siebel⁵⁰,
 A.Sisakian¹⁵, G.Smadja²⁵, O.Smirnova²⁴, A.Sokolov⁴⁰, A.Sopczak²⁰, R.Sosnowski⁴⁹, T.Spaso⁸, M.Stanitzki¹⁶,
 A.Stocchi¹⁹, J.Strauss⁴⁸, B.Stugu⁴, M.Szczekowski⁴⁹, M.Szeptycka⁴⁹, T.Szumlak¹⁸, T.Tabarelli²⁷, A.C.Taffard²²,
 F.Tegenfeldt⁴⁶, F.Terranova²⁷, J.Timmermans²⁹, N.Tinti⁵, L.Tkatchev¹⁵, M.Tobin²², S.Todorovova⁸, B.Tome²¹,
 A.Tonazzo²⁶, P.Tortosa⁴⁷, P.Travnicek²⁸, D.Treille⁸, G.Tristram⁷, M.Trochimczuk⁴⁹, C.Troncon²⁶, I.A.Tyapkin¹⁵,
 P.Tyapkin¹⁵, S.Tzamaris¹¹, O.Ullaland⁸, V.Uvarov⁴⁰, G.Valenti⁵, P.Van Dam²⁹, J.Van Eldik⁸, A.Van Lysebetten²,
 N.van Remortel², I.Van Vulpen²⁹, G.Vegni²⁶, F.Veloso²¹, W.Venus³⁵, F.Verbeure², P.Verdier²⁵, V.Verzi³⁶, D.Vilanova³⁸,

¹Department of Physics and Astronomy, Iowa State University, Ames IA 50011-3160, USA

²Physics Department, Universiteit Antwerpen, Universiteitsplein 1, B-2610 Antwerpen, Belgium
and IIHE, ULB-VUB, Pleinlaan 2, B-1050 Brussels, Belgium

and Faculté des Sciences, Univ. de l'Etat Mons, Av. Maistriau 19, B-7000 Mons, Belgium

³Physics Laboratory, University of Athens, Solonos Str. 104, GR-10680 Athens, Greece

⁴Department of Physics, University of Bergen, Allégaten 55, NO-5007 Bergen, Norway

⁵Dipartimento di Fisica, Università di Bologna and INFN, Via Irnerio 46, IT-40126 Bologna, Italy

⁶Centro Brasileiro de Pesquisas Físicas, rua Xavier Sigaud 150, BR-22290 Rio de Janeiro, Brazil

and Depto. de Física, Pont. Univ. Católica, C.P. 38071 BR-22453 Rio de Janeiro, Brazil
and Inst. de Física, Univ. Estadual do Rio de Janeiro, rua São Francisco Xavier 524, Rio de Janeiro, Brazil

⁷Collège de France, Lab. de Physique Corpusculaire, IN2P3-CNRS, FR-75231 Paris Cedex 05, France

⁸CERN, CH-1211 Geneva 23, Switzerland

⁹Institut de Recherches Subatomiques, IN2P3 - CNRS/ULP - BP20, FR-67037 Strasbourg Cedex, France

¹⁰Now at DESY-Zeuthen, Platanenallee 6, D-15735 Zeuthen, Germany

¹¹Institute of Nuclear Physics, N.C.S.R. Demokritos, P.O. Box 60228, GR-15310 Athens, Greece

¹²Dipartimento di Fisica, Università di Genova and INFN, Via Dodecaneso 33, IT-16146 Genova, Italy

¹³Institut des Sciences Nucléaires, IN2P3-CNRS, Université de Grenoble 1, FR-38026 Grenoble Cedex, France

¹⁴Helsinki Institute of Physics, HIP, P.O. Box 9, FI-00014 Helsinki, Finland

¹⁵Joint Institute for Nuclear Research, Dubna, Head Post Office, P.O. Box 79, RU-101 000 Moscow, Russian Federation

¹⁶Institut für Experimentelle Kernphysik, Universität Karlsruhe, Postfach 6980, DE-76128 Karlsruhe, Germany

¹⁷Institute of Nuclear Physics, Ul. Kawioru 26a, PL-30055 Krakow, Poland

¹⁸Faculty of Physics and Nuclear Techniques, University of Mining and Metallurgy, PL-30055 Krakow, Poland

¹⁹Université de Paris-Sud, Lab. de l'Accélérateur Linéaire, IN2P3-CNRS, Bât. 200, FR-91405 Orsay Cedex, France

²⁰School of Physics and Chemistry, University of Lancaster, Lancaster LA1 4YB, UK

²¹LIP, IST, FCUL - Av. Elias Garcia, 14-1º, PT-1000 Lisboa Codex, Portugal

²²Department of Physics, University of Liverpool, P.O. Box 147, Liverpool L69 3BX, UK

²³LPNHE, IN2P3-CNRS, Univ. Paris VI et VII, Tour 33 (RdC), 4 place Jussieu, FR-75252 Paris Cedex 05, France

²⁴Department of Physics, University of Lund, Sölvegatan 14, SE-223 63 Lund, Sweden

²⁵Université Claude Bernard de Lyon, IPNL, IN2P3-CNRS, FR-69622 Villeurbanne Cedex, France

²⁶Dipartimento di Fisica, Università di Milano and INFN-MILANO, Via Celoria 16, IT-20133 Milan, Italy

²⁷Dipartimento di Fisica, Univ. di Milano-Bicocca and INFN-MILANO, Piazza delle Scienze 2, IT-20126 Milan, Italy

²⁸IPNP of MFF, Charles Univ., Areal MFF, V Holesovickach 2, CZ-180 00, Praha 8, Czech Republic

²⁹NIKHEF, Postbus 41882, NL-1009 DB Amsterdam, The Netherlands

³⁰National Technical University, Physics Department, Zografou Campus, GR-15773 Athens, Greece

³¹Physics Department, University of Oslo, Blindern, NO-1000 Oslo 3, Norway

³²Dpto. Física, Univ. Oviedo, Avda. Calvo Sotelo s/n, ES-33007 Oviedo, Spain

³³Department of Physics, University of Oxford, Keble Road, Oxford OX1 3RH, UK

³⁴Dipartimento di Fisica, Università di Padova and INFN, Via Marzolo 8, IT-35131 Padua, Italy

³⁵Rutherford Appleton Laboratory, Chilton, Didcot OX11 0QX, UK

³⁶Dipartimento di Fisica, Università di Roma II and INFN, Tor Vergata, IT-00173 Rome, Italy

³⁷Dipartimento di Fisica, Università di Roma III and INFN, Via della Vasca Navale 84, IT-00146 Rome, Italy

³⁸DAPNIA/Service de Physique des Particules, CEA-Saclay, FR-91191 Gif-sur-Yvette Cedex, France

³⁹Instituto de Física de Cantabria (CSIC-UC), Avda. los Castros s/n, ES-39006 Santander, Spain

⁴⁰Inst. for High Energy Physics, Serpukov P.O. Box 35, Protvino, (Moscow Region), Russian Federation

⁴¹J. Stefan Institute, Jamova 39, SI-1000 Ljubljana, Slovenia and Laboratory for Astroparticle Physics,
Nova Gorica Polytechnic, Kostanjevska 16a, SI-5000 Nova Gorica, Slovenia,

and Department of Physics, University of Ljubljana, SI-1000 Ljubljana, Slovenia

⁴²Fysikum, Stockholm University, Box 6730, SE-113 85 Stockholm, Sweden

⁴³Dipartimento di Fisica Sperimentale, Università di Torino and INFN, Via P. Giuria 1, IT-10125 Turin, Italy

⁴⁴Dipartimento di Fisica, Università di Trieste and INFN, Via A. Valerio 2, IT-34127 Trieste, Italy

and Istituto di Fisica, Università di Udine, IT-33100 Udine, Italy

⁴⁵Univ. Federal do Rio de Janeiro, C.P. 68528 Cidade Univ., Ilha do Fundão BR-21945-970 Rio de Janeiro, Brazil

⁴⁶Department of Radiation Sciences, University of Uppsala, P.O. Box 535, SE-751 21 Uppsala, Sweden

⁴⁷IFIC, Valencia-CSIC, and D.F.A.M.N., U. de Valencia, Avda. Dr. Moliner 50, ES-46100 Burjassot (Valencia), Spain

⁴⁸Institut für Hochenergiephysik, Österr. Akad. d. Wissensch., Nikolsdorfergasse 18, AT-1050 Vienna, Austria

⁴⁹Inst. Nuclear Studies and University of Warsaw, Ul. Hoza 69, PL-00681 Warsaw, Poland

⁵⁰Fachbereich Physik, University of Wuppertal, Postfach 100 127, DE-42097 Wuppertal, Germany

1 Introduction

In spite of outstanding theoretical and experimental achievements, particle physicists have not been able to decide which mechanism creates mass. It is a common belief that such a mechanism will be characterised by the observation of at least a scalar particle. Whether this object is elementary (as in the SM or MSSM scenario), composite (as in the technicolor scenario), or too heavy to be observed as a particle remains uncertain.

This paper presents a systematic search for the particles predicted by the technicolor model. Section 3 briefly recalls the framework of the technicolor (TC) model and reviews the possible signals which can be observed at LEP2. Section 4 describes the direct search for technipions performed with the DELPHI detector using the data collected in 1999 and 2000. Section 5 presents complementary searches for technirho (ρ_T) production for $M_{\rho_T} < \sqrt{s}$ in the region of higher technipion masses. Section 6 summarises the combined results.

2 Data Sample

The detailed description of the DELPHI detector can be found elsewhere [1]. For the search for π_T production, the statistics of DELPHI taken in 1999 for \sqrt{s} between 192 and 202 GeV and in 2000 for \sqrt{s} between 202 and 208 GeV are used. The integrated luminosity is about 228 pb⁻¹ for data taken in 1999 and 224 pb⁻¹ for data taken in 2000. In addition, the available DELPHI $e^+e^- \rightarrow W^+W^-$ [2] and $e^+e^- \rightarrow q\bar{q}(\gamma)$ [3] cross-section measurements are used to estimate a possible contribution from technicolor production.

Simulated events are produced with the DELPHI simulation program DELSIM and are passed through the same reconstruction chain as the data. To simulate the Standard Model (SM) backgrounds, the generator EXCALIBUR [4] is used for 4-fermion final states, PYTHIA [5] for the process $e^+e^- \rightarrow q\bar{q}(+n\gamma)$, and TWOGAM [6] for two-photon interactions. The technicolor production signal is simulated using a special generator [7] included in the PYTHIA package.

3 The Technicolor scheme at LEP

The technicolor model provides an elegant scheme to generate W/Z masses. These bosons are seen as condensates of a new family of quarks (the techniquarks) which obey a QCD-like interaction with an effective scale Λ_{TC} much larger than Λ_{QCD} . It also predicts heavy (> 1 TeV) vector mesons which cannot be observed at LEP2.

It is well known, however, that this scheme encounters several problems. It cannot correctly generate fermion masses and, in its simplest version, it contradicts the LEP1 precision measurements since it gives positive contributions to the S parameter. In technicolor models with QCD-like dynamics, $S \sim 0.45$ is expected for an isodoublet of technifermions, while the precise measurements give: $S = -0.07 \pm 0.11$ [8].

Extensions [9] have been worked out which solve these problems at the price of losing predictive power. These schemes depart from the straightforward analogy with QCD, with the usual asymptotic freedom behaviour. It turns out that perturbative calculations do not work (“walking technicolor”), and therefore the theory cannot be fully tested by precision measurements.

These extensions call for a large number N_D of technidoublets [10], and therefore for additional scalar (π_T, π'_T) and vector (ρ_T, ω_T) mesons. These can be light enough to be observed at LEP2 or the Tevatron. Our searches for technicolor production assume the theoretical model given in [11].

The main ρ_T decay modes are $\rho_T \rightarrow \pi_T \pi_T, W_L \pi_T, W_L W_L, f_i \bar{f}_i$ and $\pi_T^0 \gamma$, where W_L is the longitudinal component of the W boson. For $M_{\rho_T} > 2M_{\pi_T}$ the decay $\rho_T \rightarrow \pi_T \pi_T$ is dominant, while for $M_{\rho_T} < 2M_{\pi_T}$ the decay rates depend on many model parameters. In all cases the total ρ_T width for $M_{\rho_T} < 200 \text{ GeV}/c^2$ is predicted to be of the order of 10 GeV if any of the channels $\rho_T \rightarrow \pi_T \pi_T, \pi_T W_L, W_L W_L$ is open, and below 1 GeV if all of them are closed. For ω_T the main decay modes are $\omega_T \rightarrow \pi_T \pi_T \pi_T, \pi_T \pi_T W_L$, etc. If these decay modes are forbidden kinematically, then its dominant decay is $\omega_T \rightarrow \pi_T^0 \gamma$. By analogy with QCD it is supposed that $M_{\rho_T} \simeq M_{\omega_T}$ and $M_{\pi_T^0} \simeq M_{\pi_T^\pm}$.

Following [11], technipions are assumed to decay as $\pi_T^\pm \rightarrow c\bar{b}, c\bar{s}$ and $\tau^+ \nu_\tau$; and $\pi_T^0 \rightarrow b\bar{b}, c\bar{c}$ and $\tau^+ \tau^-$. The width, ($\pi_T \rightarrow \bar{f}' f$) is proportional to $(m_f + m_{f'})^2$, therefore the b -quark is produced in $\sim 90\%$ of π_T decays. The total π_T width is less than 1 GeV. These properties are extensively used in the following.

The ρ_T coupling to the photon and Z^0 is proportional to $Q_U - Q_D$, where Q_U and Q_D are the charges of U and D techniquarks. The value $Q_U - Q_D$ has to be one to avoid triangle anomalies. Therefore, for $M_{\rho_T} < \sqrt{s}$, it can be produced on mass shell in e^+e^- interactions through the radiative return process and its production cross-section is independent of the values chosen for Q_U and Q_D . It can then be observed as a narrow resonance in the corresponding mass distribution. The radiative return production rate normalised to the point-like cross-section is given approximately by:

$$R(e^+e^- \rightarrow \rho_T(\gamma)) \simeq \ln(s/m_e^2) \frac{\rho_T^{e^+e^-}/M_{\rho_T}}{Z^{e^+e^-}/M_Z} \frac{1}{1 - M_{\rho_T}^2/s} \quad (1)$$

In addition, ω_T can also couple to e^+e^- provided $Q_U + Q_D$ is non-zero. The following always supposes that the final state $\pi_T^0 \gamma$ can be produced through both ρ_T and ω_T .

Technipions can also be produced at LEP through virtual ρ_T exchange. The analyses presented below use the off-shell processes $e^+e^- \rightarrow \rho_T^* \rightarrow (\pi_T^\pm \pi_T^\mp, \pi_T^\pm W_L^\mp)$ and $e^+e^- \rightarrow (\rho_T^*, \omega_T^*) \rightarrow \pi_T^0 \gamma$ to search for virtual ρ_T production if $M_{\rho_T} > \sqrt{s}$. The cross-sections of these processes normalised to the point-like cross-section, derived for e^+e^- interactions from equations given in [11], are:

$$R(e^+e^- \rightarrow \rho_T^* \rightarrow a^+b^-) = \frac{[|A_{eL}(s)|^2 + |A_{eR}(s)|^2] \lambda(M_a, M_b)^{3/2} C_{ab}}{8(1 - s/M_{\rho_T}^2)^2}; \quad (2)$$

$$R(e^+e^- \rightarrow (\rho_T^*, \omega_T^*) \rightarrow \pi_T \gamma) = \frac{[|C_{eL}(s)|^2 + |C_{eR}(s)|^2] \lambda(M_{\pi_T}, 0)^{3/2} \cos^2 \chi}{16(1 - s/M_{\rho_T}^2)^2} \times \frac{\alpha \cdot (Q_U + Q_D)^2 \cdot s}{\alpha_{\rho_T} \cdot M_V^2} \quad (3)$$

In these equations $a, b = \pi_T, W_L$; $C_{ab} = \cos^4 \chi$ for $\pi_T^\pm \pi_T^\mp$, $2 \cos^2 \chi \sin^2 \chi$ for $\pi_T^\pm W_L^\mp$, and $\sin^4 \chi$ for $W_L^+ W_L^-$; and the angle χ reflects the mixing between π_T and W_L with

$$\sin^2 \chi = 1/N_D \quad (4)$$

The values $A_{eL,R}$ and $C_{eL,R}$ in (2) and (3) are given by:

$$A_{eL,R}(s) = Q_e + \frac{2 \cos 2\theta_W}{\sin^2 2\theta_W} (T_{3eL,R} - Q_e \sin^2 \theta_W) B W_Z, \quad (5)$$

$$C_{eL,R}(s) = 2Q_e - \frac{2}{\sin^2 2\theta_W} (T_{3eL,R} - Q_e \sin^2 \theta_W) BW_Z, \quad (6)$$

$$BW_Z = \frac{s}{s - M_Z^2 + i\sqrt{s} \Gamma_Z}, \quad (7)$$

where $Q_e = -1$, $T_{3eL} = -1/2$, $T_{3eR} = 0$. The phase space suppression factor $\lambda(M_a, M_b)$ is:

$$\lambda(M_a, M_b) = (1 - M_a^2/s - M_b^2/s)^2 - 4M_a^2 M_b^2/s^2. \quad (8)$$

Note that for a highly virtual ρ_T contribution, even for $M_{\rho_T}^2 \rightarrow \infty$, the value of $R(e^+e^- \rightarrow \rho_T \rightarrow a^+b^-)$ remains finite. If the Z contributions are ignored, expressions (2-8) lead to $R(e^+e^- \rightarrow \rho_T \rightarrow a^+b^-) \sim \lambda(M_a, M_b)^{3/2} C_{ab}/4$, as expected for a point-like coupling of a photon to $\pi_T^+ \pi_T^-$. This correct behaviour results from our choice of the ρ_T propagator. This feature is important, as it allows LEP to be sensitive to a light π_T even if the ρ_T is very heavy.

The processes $e^+e^- \rightarrow \rho_T^* \rightarrow (\pi_T^+ \pi_T^-, \pi_T^+ W_L^-)$ depend on 3 quantities, namely M_{π_T} , M_{ρ_T} and N_D . Three additional parameters, namely the technicolor coupling constant α_{ρ_T} , the sum of charges of the technicolor doublet $Q_U + Q_D$, and the mass scale M_V are introduced to describe $e^+e^- \rightarrow (\rho_T^*, \omega_T^*) \rightarrow \pi_T^0 \gamma$. Figure 1 shows the cross-sections of processes (1-3) for some typical parameter values proposed in [11]: $M_{\pi_T} = 90$ GeV/c², $M_V = 200$ GeV/c², $N_D = 9$, $(Q_U + Q_D) = 4/3$. It is assumed that the symmetry group, under which the technifermions transform as fundamental, is $SU(N_{TC})$ with $N_{TC} = 4$ and that $\alpha_{\rho_T} = 2.91(3/N_{TC})$.

It can be seen that the production cross-section of technicolor objects is expected to be reasonably high for a wide range of M_{ρ_T} values, making the search at LEP possible, but that the process (3), giving the $\pi_T^0 \gamma$ final state, depends strongly on the three additional parameters, and can even become zero for $(Q_U + Q_D) = 0$.

This paper reports searches for ρ_T with $M_{\rho_T} < \sqrt{s}$ in all decay modes in process (1), for $\pi_T^+ \pi_T^-$ and $\pi_T^+ W_L^-$ final states in process (2), and for $\pi_T \gamma$ in process (3). It is assumed that $M_{\rho_T} > 90$ GeV/c² and $M_{\pi_T} > 45$ GeV/c², supposing that the ρ_T and π_T with smaller masses would be detected in precise measurements at LEP1. The CDF experiment at the Tevatron [12] has already published results of a search for these particles.

4 Search for π_T in $e^+e^- \rightarrow \rho_T^* \rightarrow (W_L \pi_T, \pi_T \pi_T)$

If the π_T is light enough, $W_L^+ \pi_T^-$ or even $\pi_T^+ \pi_T^-$ final states can be produced in process (2). These can provide striking signatures because technipions are expected [11] to decay into the heaviest fermions. Charged technipions therefore prefer final states with a b quark, which can be separated from the W bosons by applying b-tagging.

4.1 Search in the 4-jet Final State

Events originating from the signal contain mainly one or two b-quarks and one or two c-quarks, while the background from W^+W^- contains very few b-quarks. This situation is similar to that in the Higgs search in 4 jet final states, therefore the same jet clustering algorithm using the DURHAM method [13] and the same b-tagging procedure [14] are applied. The analysis starts with the four-jet preselection described in [15], which aims to eliminate the radiative and $\gamma\gamma$ events and to reduce the QCD and $Z^0 \gamma^*$ background.

The $q\bar{q}(\gamma)$ and 4-fermion backgrounds remaining after the preselection have to be reduced further. For this purpose different shape and b-tagging variables have been investigated, assuming that the analysis should be sensitive and keep a reasonable efficiency for a wide range of the π_T mass from $\sim 45 \text{ GeV}/c^2$ up to the kinematical limit.

Finally, 12 variables are selected for this analysis and the final discriminant variable is defined as the output of a neural network (NN). There are two b-tagging variables intended to reduce the W^+W^- background: one of them (x_b) is computed as the sum of the two highest jet b-tagging variables [16], and the other is the sum of the four jet b-tagging variables. Seven shape variables are used to reduce the $q\bar{q}(\gamma)$ contamination. They are the sum of the second and fourth Fox-Wolfram moments, the product of the minimum jet energy and the minimum opening angle between any two jets, the event thrust, the sum of the four lowest angles between any pair of jets in the event, the minimal di-jet mass, and the minimal y_{cut} values for which the event is clustered into 4 jets (y_{34}) and into 5 jets (y_{45}). Finally, three more variables take into account the two-boson event topology. To define them the event is forced into four jets, a five constraint fit requiring conservation of energy and momentum and equal masses of opposite jet pairs is applied to all possible jet pairings, and the pairing giving the smallest value of the fit χ_{5C}^2 is selected. The variables then included in the neural network are the smallest χ_{5C}^2 , the production angle of the jet pair, and the angle between the planes defined by the two jet pairs.

The resulting NN output provides good background suppression and high selection efficiency over a wide range of M_{π_T} . As an example, Table 1 gives the $\pi_T\pi_T$ and $W_L\pi_T$ efficiencies for different π_T masses obtained when selecting events with NN output > 0.3 .

The distributions of some discriminating variables for data, the SM prediction, and technipion production are shown in Fig. 2. The mass M_{5C} of the jet pair after the 5C fit for the pairing with the smallest χ_{5C}^2 is used as the π_T mass estimator. Figure 3 shows its distribution for preselected events, for the Standard Model (SM) background sources, and for technipion production with $M_{\pi_T} = 99 \text{ GeV}/c^2$. The possible contribution of $\pi_T\pi_T$ production would be seen as a narrow peak. The channel $W_L\pi_T$ would give a slightly wider peak shifted towards the mass of the W. The form of the mass spectrum of the sum of these two channels depends on the ρ_t mass and the mixing angle χ (see Eq. (2)). This figure also shows the distribution of the final discriminant variable from the neural network output. Figure 4 shows the number of selected events as a function of the efficiency for a $\pi_T\pi_T$ signal, which is varied by changing the cut on the NN output. The dependence is shown separately for the two years of data taking used. Figure 5 shows the M_{5C} mass spectrum for events with the NN output greater than 0.30 for the full statistics collected at $\sqrt{s} = 192 - 208 \text{ GeV}$. A reasonable agreement between data and the SM prediction is observed in all distributions, the remaining differences are included in the systematic errors.

Figure 5 also shows the expected spectrum of $W_L\pi_T$ and $\pi_T\pi_T$ production for $M_{\pi_T} = 99 \text{ GeV}/c^2$, $M_{\rho_T} = 220 \text{ GeV}/c^2$ and $N_D = 9$ normalised to the collected luminosity. For these model parameters the signal to background ratio for events with $M_{5C} > 96 \text{ GeV}/c^2$ is about 6.

In addition to the NN analysis, a sequential analysis was also developed. Its performance is slightly worse, and therefore it is used only as a cross-check. After the preselection stage it uses three discriminating variables. Two of them are intended to reduce the $q\bar{q}(\gamma)$ contamination. They are y_{34} , defined above, and the sum of the second and fourth Fox-Wolfram moments, $H_2 + H_4$. Events are required to have $y_{34} > 0.003$

and $H_2 + H_4 < 0.6$. The cut on the b-tagging variable $x_b > 1.3$ is used to suppress the W^+W^- background.

Tables 2 and 3 give the numbers of selected and expected events at different steps of the sequential analysis together with the efficiency of the signal selection. For comparison, the results of the NN analysis for NN output cuts giving similar signal efficiencies are also shown. The results of both analyses show good agreement of the data with the SM prediction. No contribution from technicolor production is observed.

channel	M_{π_T} (GeV/c ²)							
	50	60	70	80	90	99	100	110
$W_L\pi_T$	7.9	9.5	11.0	11.5	12.9		14.6	13.9
$\pi_T\pi_T$	23.7	32.9	33.9	36.0	42.5	49.6		

Table 1: Search in the 4-jet final state: selection efficiency in percent (including topological branching ratios) for $W_L\pi_T$ and $\pi_T\pi_T$ for different π_T masses M_{π_T} , $\sqrt{s} = 200$ GeV, and NN output variable > 0.3 .

Selection	Data	Total background	q \bar{q} (γ)	4 fermion	Efficiency $\pi_T\pi_T$ (%)	Efficiency $W_L\pi_T$ (%)
Preselection	2455	2471.4	751.7	1719.7	93.4	62.5
$y_{34} \geq 0.003$	2035	2042.4	460.3	1582.1	90.0	58.6
$H_2 + H_4 \leq 0.6$	1459	1488.1	178.2	1309.9	78.5	51.7
$x_b \geq 1.3$	48	50.0	20.8	29.2	43.9	14.3
NN > 0.3	32	37.6	12.4	25.2	42.5	12.9

Table 2: Search in the 4-jet final state: effect of the selection cuts in the sequential analysis on data, simulated background and simulated signal events at $\sqrt{s} = 192$ -202 GeV. Efficiencies are given for $M_{\pi_T} = 90$ GeV/c² and include the topological branching ratios of W and π_T to two jets.

Selection	Data	Total background	q \bar{q} (γ)	4 fermion	Efficiency $\pi_T\pi_T$ (%)	Efficiency $W_L\pi_T$ (%)
Preselection	2266	2342.1	680.3	1661.8	91.1	64.9
$y_{34} \geq 0.003$	1929	1940.7	416.8	1523.8	89.3	60.7
$H_2 + H_4 \leq 0.6$	1368	1395.6	163.0	1232.7	72.8	52.6
$x_b \geq 1.3$	43	46.4	18.1	28.3	44.9	13.7
NN > 0.34	29	30.2	9.3	20.9	45.0	11.0

Table 3: Search in the 4-jet final state: effect of the selection cuts in the sequential analysis on data, simulated background and simulated signal events at $\sqrt{s} = 204$ -208 GeV. Efficiencies are given for $M_{\pi_T} = 99$ GeV/c² and include the topological branching ratios of W and π_T to two jets.

4.2 Search in the Semileptonic Final State

The search for the technipion is also performed in channels containing two quarks, a lepton and a neutrino, corresponding to the decays $W_L^+ \pi_T^- \rightarrow l^+ \nu q \bar{q}$ and $\pi_T^+ \pi_T^- \rightarrow \tau \bar{\nu} q \bar{q}$. This final state is selected in two steps.

Since the topology searched for is very close to that of semileptonic W^+W^- decays, a similar selection [2] is applied at the first step. However, variables strongly correlated with the boson mass are not used, making the analysis efficient for a wide range of π_T^- masses.

Firstly loose initial cuts, requiring at least 7 charged particles, transverse energy greater than $0.25\sqrt{s}$, less than 30 GeV in a 30° cone around the beam, and the polar angle of the missing momentum fulfilling $|\cos \theta_{miss}| < 0.985$, are used to remove a large fraction of the leptonic, $q\bar{q}(\gamma)$ and $\gamma\gamma$ events.

Then an isolated lepton candidate has to be found. The isolation criterion is defined in terms of the product $p \cdot \theta_{iso}$, where p is the lepton momentum and θ_{iso} is the isolation angle between the lepton and the nearest charged particle with momentum greater than 1 GeV/c. Electrons and muons are identified using the standard DELPHI tools [1] and $p \cdot \theta_{iso}$ is required to be above 250 GeV/c-degrees. Any other isolated electron or muon with energy between 5 and 25 GeV or an isolated charged hadron or low multiplicity jet (less than 5 charged particles) is identified as a τ -lepton candidate. For these, since some part of the tau energy is taken away by neutrinos, the isolation requirement is relaxed to $p \cdot \theta_{iso} > 150$ GeV/c-degrees.

Depending on the flavour of the isolated lepton candidate, different neural networks are then used to reduce the background further. For a muon candidate, a neural network with 7 input variables is used: the lepton momentum, lepton isolation, missing momentum, $|\cos \theta_{miss}|$, transverse momentum, visible energy, and $\sqrt{s'/s}$ where s' is the reconstructed effective centre-of-mass energy [17]. One more variable, the acoplanarity angle¹ between the lepton and the hadronic system, is used for an electron. For tau candidates, the missing momentum and visible energy are less discriminant and are replaced by four new variables: the thrust, the angle between the lepton and hadronic system, and the acoplanarity and acollinearity of the hadronic jets. The neural network outputs for the different leptons are shown in Figure 6. The events are accepted if the NN value is above 0.4 for electrons and muons and above 0.6 for taus. In this way most of the non- W^+W^- background is rejected.

The second step exploits the specific properties of the signal, such as the presence of b-quarks or the production angle, to distinguish it from the W pairs. This is done using another neural network which uses four input variables: the b -tagging variables of the two hadronic jets, $q \cdot \cos \theta_{prod}$ and $|\cos \theta_{miss}|$. The charge q is defined according to that of the lepton, and the production polar angle θ_{prod} is built from the hadronic jets. The distribution of the b -tagging variable and $q \cdot \cos \theta_{prod}$, together with the NN output are shown in Figure 7.

This analysis provides good background suppression and a reasonable selection efficiency of the $W_L \pi_T$ final state. The $\pi_T \pi_T$ efficiency is limited by the small $\pi_T \rightarrow \tau \bar{\nu}$ decay rate. Table 4 gives the $\pi_T \pi_T$ and $W_L \pi_T$ efficiencies for different M_{π_T} masses obtained when selecting events with NN output > 0.1 .

The M_{π_T} mass estimator is the same as in the hadronic channel. The constrained fit is done with three additional free parameters coming from undetected neutrino for electron and muon, and with four parameters for tau, since also its energy is not known.

¹For any two vectors the acoplanarity is defined as the angle between their projections on the plane perpendicular to the beam direction.

Figure 8 shows the π_T mass spectrum for events with the NN output greater than 0.1 for the full statistics collected at $\sqrt{s}=192\text{-}208$ GeV. This figure also shows the expected spectrum of $W_L\pi_T$ and $\pi_T\pi_T$ production for $M_{\pi_T}=100$ GeV/ c^2 , $M_{\rho_T}=220$ GeV/ c^2 and $N_D = 9$ normalised to the collected luminosity. A good agreement between data and the SM prediction is observed.

Table 5 gives the number of selected and expected events at different steps of analysis and for several cuts on the NN output. No contribution from technicolor production is observed.

channel	M_{π_T} (GeV/ c^2)								
	50	60	70	80	90	99	100	110	120
$W_L\pi_T$	12.4	11.5	12.5	14.1	14.1		12.9	11.9	10.4
$\pi_T\pi_T$	2.0	2.6	2.7	3.0	2.9	2.2			

Table 4: Search in the semileptonic final state: Selection efficiency in percent (including topological branching ratios) for π_TW_L and $\pi_T\pi_T$ for different π_T masses M_{π_T} , $\sqrt{s} = 200$ GeV, and NN output > 0.1 .

Selection	Data	Total background	$WW \rightarrow q\bar{q}l\nu$	$q\bar{q}(\gamma)$	Efficiency $W_L\pi_T$ (%)
Hadronic preselection	19994	19626.1	2952.9	12446.3	96.9%
$q\bar{q}l\nu$ selection	2375	2504.9	2309.1	63.1	23.5%
NN output > 0.1	81	76.9	54.9	7.4	12.9%
NN output > 0.2	32	33.2	18.8	5.3	10.4%
NN output > 0.3	17	18.9	8.2	4.1	7.4%

Table 5: Search in the semileptonic final state: Effect of the selection cuts on data, simulated background and simulated signal events at $\sqrt{s} = 192\text{-}208$ GeV. Efficiencies are given for $\pi_TW_L \rightarrow bcW_L$ with $M_{\pi_T} = 100$ GeV/ c^2 .

4.3 Combined result of the π_T search

Since good agreement between data and the Standard Model expectation is observed, the results are used to set limits on technicolor production, which are presented as a 95% CL exclusion region in the (M_{ρ_T}, M_{π_T}) plane. The observed and expected limits quoted are based on the confidence level for signal, CL_s , as described in [18]. The test statistic used is a likelihood ratio, based on comparing the observed and expected rates and distributions as a function of mass and NN output. The statistical and systematic errors on the expected background and signal distributions are taken into account.

In the four-jet channel the relative systematic error was estimated at 11% in the background level and 5% in the signal efficiency. The main contribution, evaluated at about 10% in the background and at 4% in the signal efficiency, comes from the b -tagging. In the semileptonic channel the main uncertainty is related to the lepton identification efficiency. The total relative error is estimated at 10% in the background and 2% in the signal efficiency.

The $\pi_T\pi_T \rightarrow \tau\bar{\nu}q\bar{q}$ channel was not included in the limits estimate, because its selection efficiency is significantly less than in the $\pi_T\pi_T \rightarrow q\bar{q}q\bar{q}$ channel, see tables 1,4.

Two cases are considered separately, $N_D = 2$ (maximal mixing), see Fig. 9, and $N_D = 9$ (theoretically preferred [11]), see Fig. 10. The regions excluded by this analysis are shown by the diagonal hatching.

In the limit of infinite ρ_T mass and assuming a point-like coupling of the gauge bosons to $\pi_T^\pm \pi_T^\mp$, the DELPHI data set 95% CL lower limits on the charged technipion mass of $M_{\pi_T} = 79.8 \text{ GeV}/c^2$ ($81.1 \text{ GeV}/c^2$ expected) for $N_D = 2$, and $M_{\pi_T} = 89.1 \text{ GeV}/c^2$ ($88.1 \text{ GeV}/c^2$ expected) for $N_D = 9$.

Although the limit on the π_T mass excludes a technicolor interpretation of the excess of events observed by L3 [19] at $68 \text{ GeV}/c^2$ in their H^+H^- analysis, it should be noted that the DELPHI mass limit was obtained by applying b -tagging and therefore the present analysis cannot be compared directly with the L3 result.

Relaxing the hypothesis of a dominant technipion decay into b quarks, used in this analysis, will not drastically modify the obtained result for $N_D=9$. In this case the $\pi_T^\pm \pi_T^\mp$ channel, when the ρ_T becomes very heavy, has almost the same cross-section as the H^+H^- channel of MSSM. Therefore, the results of H^+H^- search [20], which give a limit just below the W mass, can also be used to set a limit on the technipion production. However, for $N_D=2$ the drop in production cross-section is significant and a special analysis is required.

5 Search for ρ_T with $M_{\rho_T} < \sqrt{s}$

A ρ_T with mass below \sqrt{s} can be produced on mass shell in the radiative return process $e^+e^- \rightarrow \rho_T(\gamma)$ with subsequent decay into different final states. This section presents the search for ρ_T in all the main ρ_T decay modes in the M_{π_T} region not covered by the results of the section 4. It is based on a special search for the $\pi_T\gamma$ channel and on previous DELPHI measurements [2,3] of the WW and $q\bar{q}$ production cross-sections.

5.1 $e^+e^- \rightarrow \rho_T(\gamma)$ with $\rho_T \rightarrow \pi_T^0\gamma$

The decay $\rho_T \rightarrow \pi_T^0\gamma$ is more favourable kinematically than charged π_T pair production and the dominant decay of π_T^0 into $b\bar{b}$ ($\sim 90\%$) allows a clean experimental signature. There is also an isosinglet called $\pi_T^{\prime 0}$ which can decay into gluons and fermions and is expected to have about the same mass. To be conservative, its possible contribution is ignored.

The hadronic events are selected by requiring at least 6 charged particles with a total energy exceeding 24% of the centre-of-mass energy. Any photon with an energy exceeding 5 GeV is considered as a possible isolated photon candidate. All the other particles in the event are clustered into jets using the JADE algorithm [5], and the photon is accepted as isolated if either its transverse momentum to the nearest jet exceeds 10 GeV/c or the angle between its direction and the nearest jet exceeds 45 degrees. More than one isolated photon is allowed in an event.

A constrained fit requiring the conservation of energy and momentum and allowing one additional photon in the beam pipe is then applied to all selected events. An event is rejected if the χ^2 of this fit exceeds 9. The sum of all particles excluding the isolated photons is called the hadronic system. The momentum of the hadronic system computed after the constrained fit is required to exceed 10 GeV/c, and the polar angle of its direction Θ_{had} to satisfy the condition $|\cos \Theta_{had}| < 0.9$. The reconstructed hadronic system is combined with the isolated photon, which is required to have $|\cos \Theta_\gamma| < 0.98$ where

Θ_γ is the polar angle of its direction. The energy of the combined (hadronic+photon) system is required to be less than $\sqrt{s} - 5$ GeV, assuming at least one additional photon with energy above 5 GeV. Finally, as the main π_T^0 decay mode should be $\pi_T^0 \rightarrow b\bar{b}$, the b-tagging variable for the event x_b , defined in section 4.1, is required to exceed -1 . The QCD background remaining after this cut has a b -purity of about 77%.

With these selections 156 events are observed in the statistics collected in 1999 and 2000 while 149.9 events are expected from the different SM sources. Figure 11a shows the $(q\bar{q}\gamma)$ mass distribution of all selected events. The production of ρ_T should manifest itself as a peak both in the distribution of the hadronic mass, corresponding to the π_T^0 , and in the mass of the hadronic system plus photon, corresponding to the ρ_T , while no contribution from $\rho_T \rightarrow \pi_T^0\gamma$ is seen in Fig. 11a. A 15% systematic error is assigned, which takes into account the uncertainty in the selection efficiency of $b\bar{b}\gamma(\gamma)$ events (10%) and uncertainty in the standard model cross-section $e^+e^- \rightarrow q\bar{q}\gamma(\gamma)$ (11%). Within the framework of the model [11], the resulting 95% CL upper limit on the branching ratio $BR(\rho_T \rightarrow \pi_T^0\gamma)$ does not exceed 7% for $90 < M_{\rho_T} < 202$ GeV/c².

Due to this upper limit on $BR(\rho_T \rightarrow \pi_T^0\gamma)$, the other decay modes ($\rho_T \rightarrow W_L W_L$, $q\bar{q}$, $\pi_T\pi_T$) must dominate. The search for these channels is presented in the following sections.

In addition, the $\pi_T\gamma$ system can be produced in process (3), even if $M_{\rho_T} > \sqrt{s}$. The topology of this process is different, and therefore the condition that the energy of the (hadronic+photon) system is at least 5 GeV below \sqrt{s} is not applied. Dropping this condition, 468 events are selected in data and 502.6 events are expected from the standard sources. The distribution of the hadronic mass for this selection is shown in Fig. 11b, where only the expected Z^0 peak from the radiative return process is observed.

The exclusion region in the (M_{ρ_T}, M_{π_T}) plane coming from the search for $e^+e^- \rightarrow (\rho_T^*, \omega_T^*) \rightarrow \pi_T^0\gamma$ production is strongly model dependent and can even completely disappear for $Q_U + Q_D = 0$ (see eq. 3). In addition, for the typical parameter values, the extension of the limit given by other channels is rather small. Therefore, the results of the $e^+e^- \rightarrow (\rho_T^*, \omega_T^*) \rightarrow \pi_T^0\gamma$ search are not included in the exclusion region given in Figs. 9,10.

5.2 $e^+e^- \rightarrow \rho_T(\gamma)$ with $\rho_T \rightarrow W_L W_L$

This section presents the search for the $\rho_T \rightarrow W_L W_L$ decay with the ρ_T mass above the $2M_W$ threshold. It supposes that the M_{π_T} value is not excluded by the analysis of section 4 (see Figs. 9, 10), i.e. that the channels $\rho_T \rightarrow W_L\pi_T$, $\pi_T\pi_T$ are kinematically closed.

The search for this decay uses the DELPHI measurement of the W^+W^- cross-section at $\sqrt{s} = 172 - 206.7$ GeV [2], which applies no strong condition on the energy of any ISR photon. Figure 12 shows the resulting stability of the selection efficiency over wide ranges of $M_{W^+W^-}/\sqrt{s}$ for both the $q\bar{q}q\bar{q}$ and $q\bar{q}l\bar{\nu}$ final states. Therefore the decay mode $\rho_T \rightarrow W_L W_L$ would give an additional contribution to the W^+W^- cross-section.

The measured values of the W^+W^- cross-section are taken from [2]. The Standard Model prediction is computed using the RacoonWW generator [21], while the selection efficiency is computed using EXCALIBUR [4]. An additional 2% systematic uncertainty is assigned to take into account a possible impact on the selection efficiency of differences in the event topology between these two generators. This analysis conservatively supposes all systematic errors to be fully correlated. The expected cross-section of $e^+e^- \rightarrow \rho_T(\gamma)$ for some specific ρ_T mass values is given in Table 6. The precision of W^+W^- cross-section

M_{ρ_T} (GeV/c ²)	\sqrt{s} (GeV)							
	183	189	192	196	200	202	205	207
175	7.00	4.39	3.69	3.03	2.57	2.38	2.15	2.01
185	–	10.68	7.25	5.06	3.87	3.45	2.97	2.71
195	–	–	–	18.82	8.69	6.83	5.15	4.42

Table 6: Expected $e^+e^- \rightarrow \rho_T(\gamma)$ cross-section (in pb) at different centre-of-mass energies for some ρ_T mass values.

measurement is significantly better, e.g. DELPHI reported $\sigma = 15.83 \pm 0.38 \pm 0.20$ pb at $\sqrt{s} = 189$ GeV and the expected Standard Model value is 16.25 pb.

No additional statistically significant contribution to the W^+W^- cross-section is observed for any centre-of-mass energy. Instead, the available measurements of the W^+W^- cross-section put a 95% CL upper limit on the branching ratio $BR(\rho_T \rightarrow W^+W^-)$. It depends on the ρ_T mass but in all cases is below 30%. Since $BR(\rho_T \rightarrow \pi_T^0\gamma)$ is limited to 7% at 95% CL (see section 5.1), the decay $\rho_T \rightarrow W_LW_L$ must be dominant in the (M_{ρ_T}, M_{π_T}) mass region considered. Therefore, the result obtained excludes ρ_T production for all M_{ρ_T} between $2M_W$ and 206.7 GeV/c² and for all M_{π_T} not excluded by the analysis of section 4. The region in the (M_{ρ_T}, M_{π_T}) plane excluded by this analysis is shown by the vertical hatching in Figs. 9,10.

5.3 $e^+e^- \rightarrow \rho_T(\gamma)$ with $\rho_T \rightarrow$ hadrons ($q\bar{q}, \pi_T\pi_T$)

For $M_{\rho_T} < \sqrt{s}$, technicolor production by process (1) would give a significant contribution to the cross-section for $q\bar{q}(\gamma)$ production because the main ρ_T decay channels all include hadronic final states. Due to the relatively small ρ_T decay width, this contribution would be observed as a peak in the hadronic mass distribution. The search for this decay channel uses all published DELPHI $q\bar{q}(\gamma)$ cross-section measurements, which are currently available for $\sqrt{s} = 183$ and 189 GeV [3], and is limited to ρ_T mass values below 165 GeV/c². Above 165 GeV/c² either the decay $\rho_T \rightarrow W_LW_L$, considered in section 5.2, or the decays $\rho_T \rightarrow (\pi_T\pi_T, W_L\pi_T)$, considered in section 4, become dominant.

The topology of $\rho_T \rightarrow q\bar{q}$ events is almost the same as that of standard $e^+e^- \rightarrow q\bar{q}(\gamma)$ processes, while the decay $\rho_T \rightarrow \pi_T\pi_T$ produces many-jet events. However, the $q\bar{q}(\gamma)$ selection criteria [3] are quite loose, allowing effective selection of both ρ_T decay modes. This was verified by passing simulated $e^+e^- \rightarrow \rho_T(\gamma) \rightarrow \pi_T\pi_T(\gamma)$ events through the complete $q\bar{q}(\gamma)$ analysis chain. The selection efficiency was found to be the same as for standard $q\bar{q}(\gamma)$ events.

Figure 13a shows the observed mass distribution of the hadronic system together with the expected contribution from Standard Model processes. The hadronic mass reconstruction is described in [3]. Figure 13b shows the difference between the observed and expected numbers of events and the contribution of a $\rho_T \rightarrow \pi_T\pi_T$ signal with $M_{\rho_T} = 150$ GeV/c² and $M_{\pi_T} = 70$ GeV/c². Good sensitivity to technicolor production can be seen.

Using the observed and expected numbers of events gives the 95% CL upper limit on the decay branching ratio $BR(\rho_T \rightarrow \text{hadrons})$ shown in Fig. 13c. The small mismatch between data and simulation for the width of the radiative return to the Z^0 in Fig. 13a is due to imprecise modeling of such details as jet angles and momenta. It explains some increase of the $BR(\rho_T \rightarrow \text{hadrons})$ limit around 100 GeV, which, however, remains below 55%. Taking into account that $BR(\rho_T \rightarrow \pi_T^0\gamma)$ is limited by 7% at 95% CL (see sec. 5.1),

this result excludes ρ_T production for all ρ_T masses between 90 and 165 GeV/ c^2 . The horizontal hatching in Figs. 9, 10 show the contribution of this channel in the combined excluded region in the (M_{ρ_T}, M_{π_T}) plane.

6 Summary

This paper presented the search for $\pi_T\pi_T$ and $W_L\pi_T$ production in process (2) and for ρ_T production in the radiative return process (1) followed by the decays $\rho_T \rightarrow \pi_T^0\gamma$, $\rho_T \rightarrow W^+W^-$ or $\rho_T \rightarrow \text{hadrons}$. A good agreement between data and the Standard Model expectation is observed in all channels studied. The combined region in the (M_{ρ_T}, M_{π_T}) plane excluded by this analysis at a 95% CL is shown in Figs. 9,10. A 95% CL lower mass limit of 79.8 GeV/ c^2 is set independently of other parameters of the technicolor model, supposing its point-like coupling with gauge bosons (see section 4.3). The ρ_T production is excluded at 95% CL for $90 < M_{\rho_T} < 206.7$ GeV/ c^2 independently of the π_T mass and all other model parameters.

These results significantly improve on the exclusion limits on technicolor production obtained by the CDF experiment [12].

Acknowledgements

We wish to thank K.Lane for answering many questions on technicolor models and encouraging this work.

We are greatly indebted to our technical collaborators, to the members of the CERN-SL Division for the excellent performance of the LEP collider, and to the funding agencies for their support in building and operating the DELPHI detector.

We acknowledge in particular the support of

Austrian Federal Ministry of Education, Science and Culture, GZ 616.364/2-III/2a/98,
FNRS-FWO, Flanders Institute to encourage scientific and technological research in the industry (IWT), Belgium,

FINEP, CNPq, CAPES, FUJB and FAPERJ, Brazil,

Czech Ministry of Industry and Trade, GA CR 202/99/1362,

Commission of the European Communities (DG XII),

Direction des Sciences de la Matière, CEA, France,

Bundesministerium für Bildung, Wissenschaft, Forschung und Technologie, Germany,

General Secretariat for Research and Technology, Greece,

National Science Foundation (NWO) and Foundation for Research on Matter (FOM),

The Netherlands,

Norwegian Research Council,

State Committee for Scientific Research, Poland, SPUB-M/CERN/PO3/DZ296/2000
and SPUB-M/CERN/PO3/DZ297/2000

JNICT-Junta Nacional de Investigação Científica e Tecnológica, Portugal,

Vedecka grantova agentura MS SR, Slovakia, Nr. 95/5195/134,

Ministry of Science and Technology of the Republic of Slovenia,

CICYT, Spain, AEN99-0950 and AEN99-0761,

The Swedish Natural Science Research Council,

Particle Physics and Astronomy Research Council, UK,

Department of Energy, USA, DE-FG02-94ER40817,

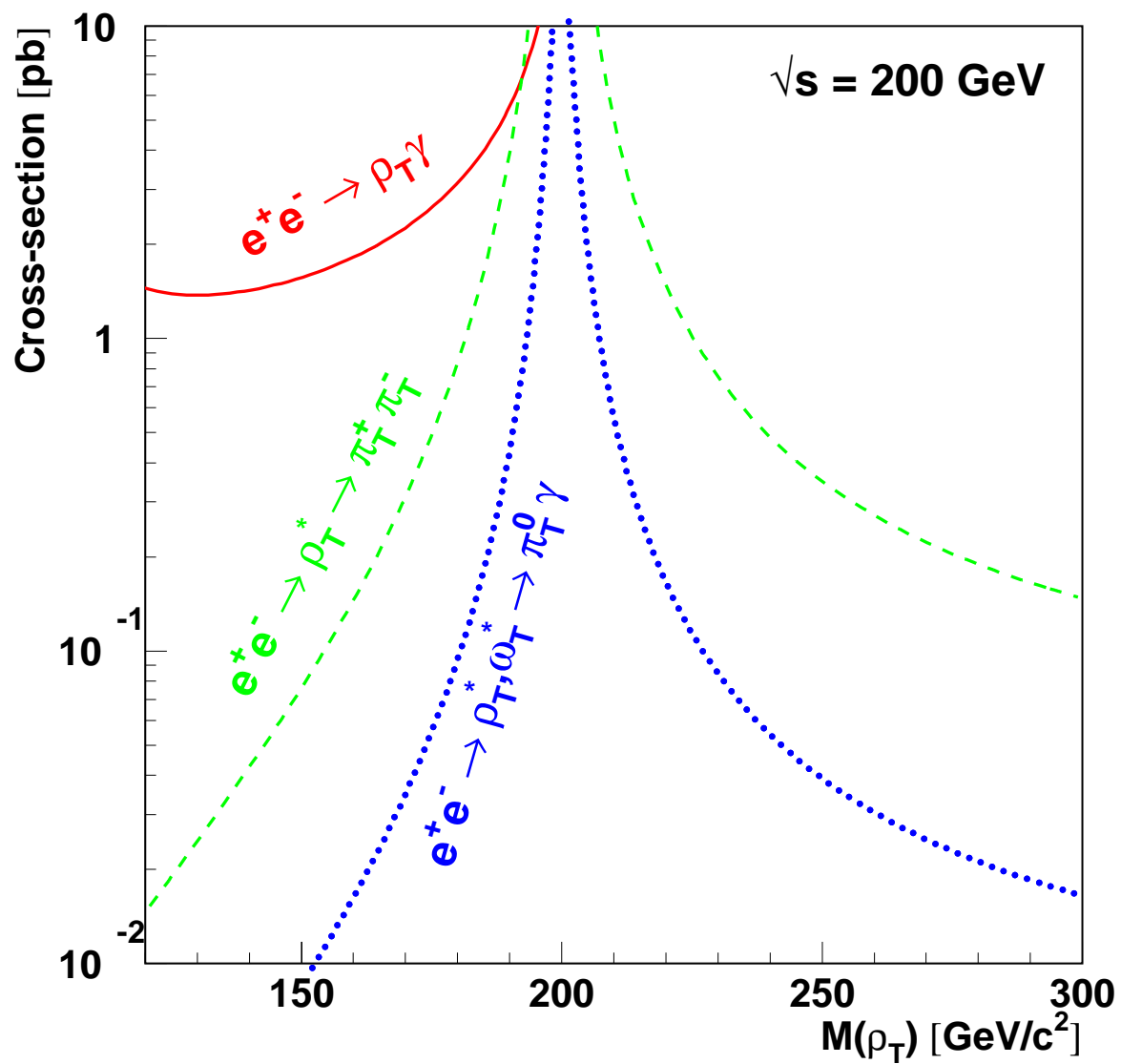


Figure 1: Technicolor production cross-sections at LEP for some typical parameter values: $M_{\pi_T} = 90 \text{ GeV}/c^2$, $M_V = 200 \text{ GeV}/c^2$, $N_D = 9$, $(Q_U + Q_D) = 4/3$, and $\alpha_{\rho_T} = 2.91(3/N_{TC})$ with $N_{TC} = 4$.

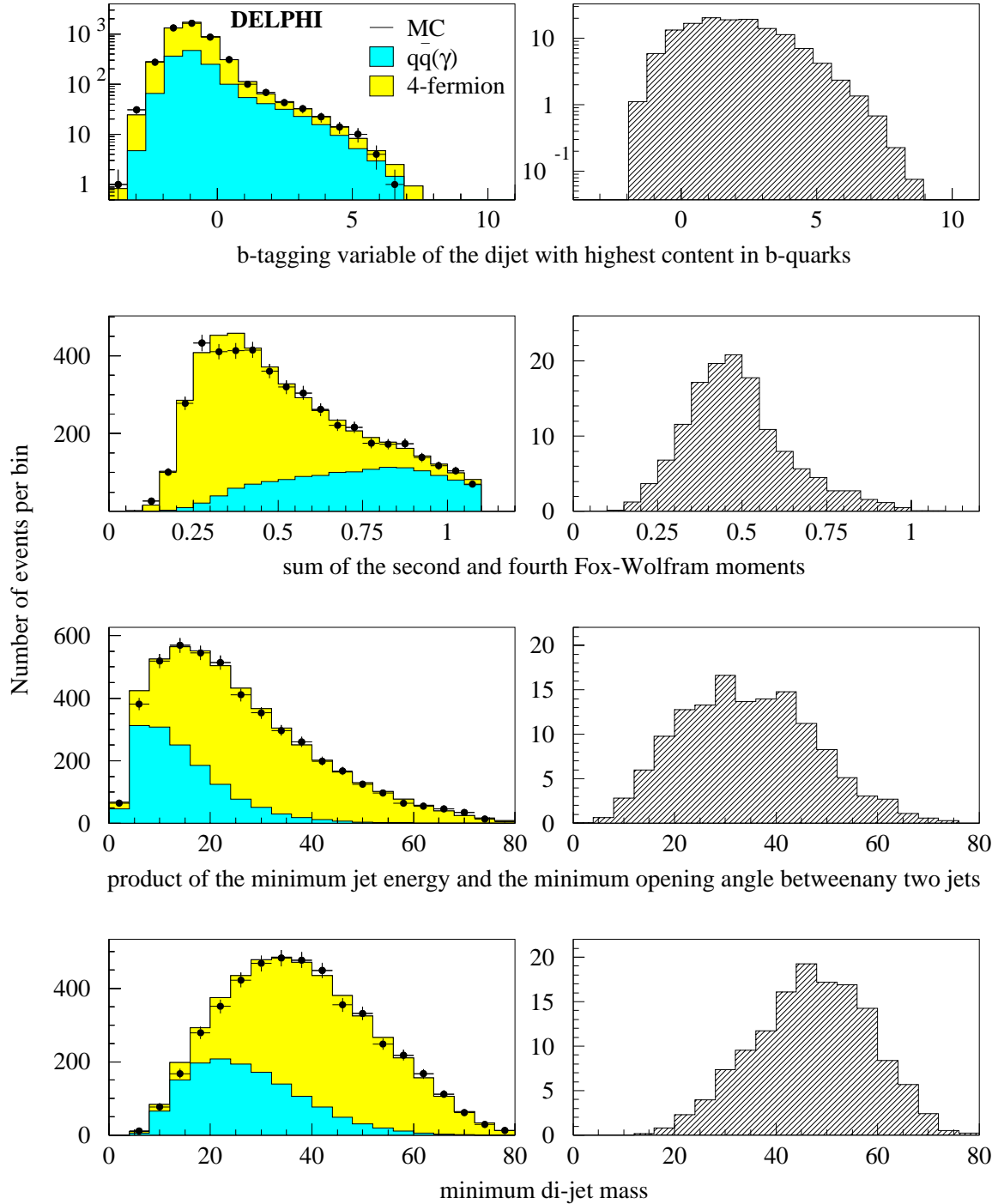


Figure 2: Search in the 4-jet final state: distributions after preselection of the b-tagging variable, $H_2 + H_4$, the product of the minimum jet energy and the minimum opening angle between any two jets. The plots on the left show the data (points) and the expected SM backgrounds (histograms) for the full DELPHI statistics at $\sqrt{s} = 192 - 208$ GeV. Those on the right show the technicolor signal expected in the channel $e^+e^- \rightarrow \pi_T\pi_T$ if $M_{\pi_T} = 99$ GeV/ c^2 . The signal normalisation corresponds to $M_{\rho_T} = 220$ GeV/ c^2 , $N_D = 9$ and the integrated luminosity collected at $\sqrt{s}=192-208$ GeV.

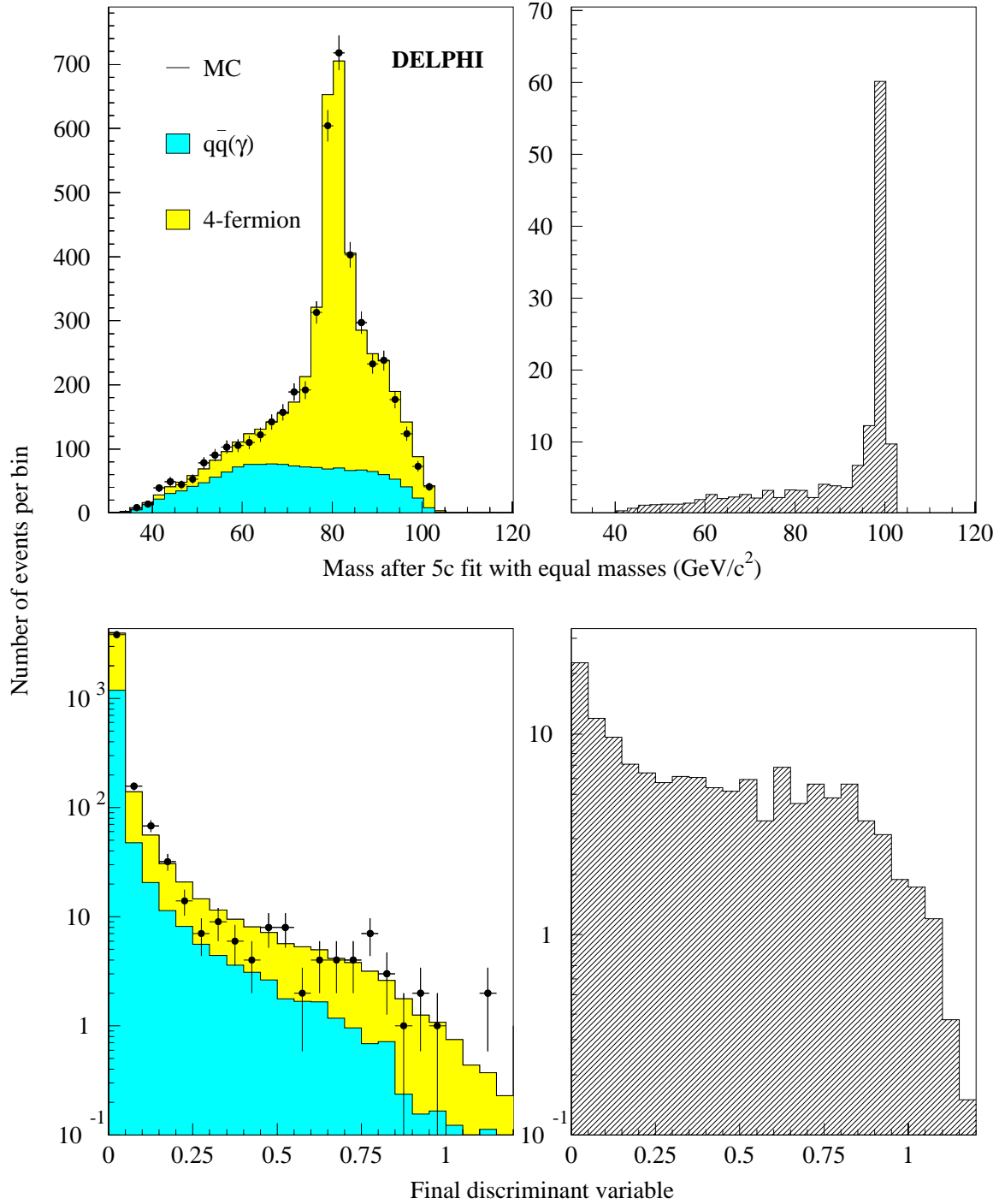


Figure 3: Search in the 4-jet final state: distributions of the mass and final discriminant variable after preselection. The plots on the left show the data (points) and the expected SM backgrounds (histograms) for the full DELPHI statistics at $\sqrt{s} = 192 - 208$ GeV. Those on the right show the technicolor signal in $e^+e^- \rightarrow \pi_T\pi_T$ expected if $M_{\pi_T} = 99$ GeV/ c^2 . The signal normalisation corresponds to $M_{\rho_T} = 220$ GeV/ c^2 , $N_D = 9$ and the integrated luminosity collected at $\sqrt{s}=192-208$ GeV.

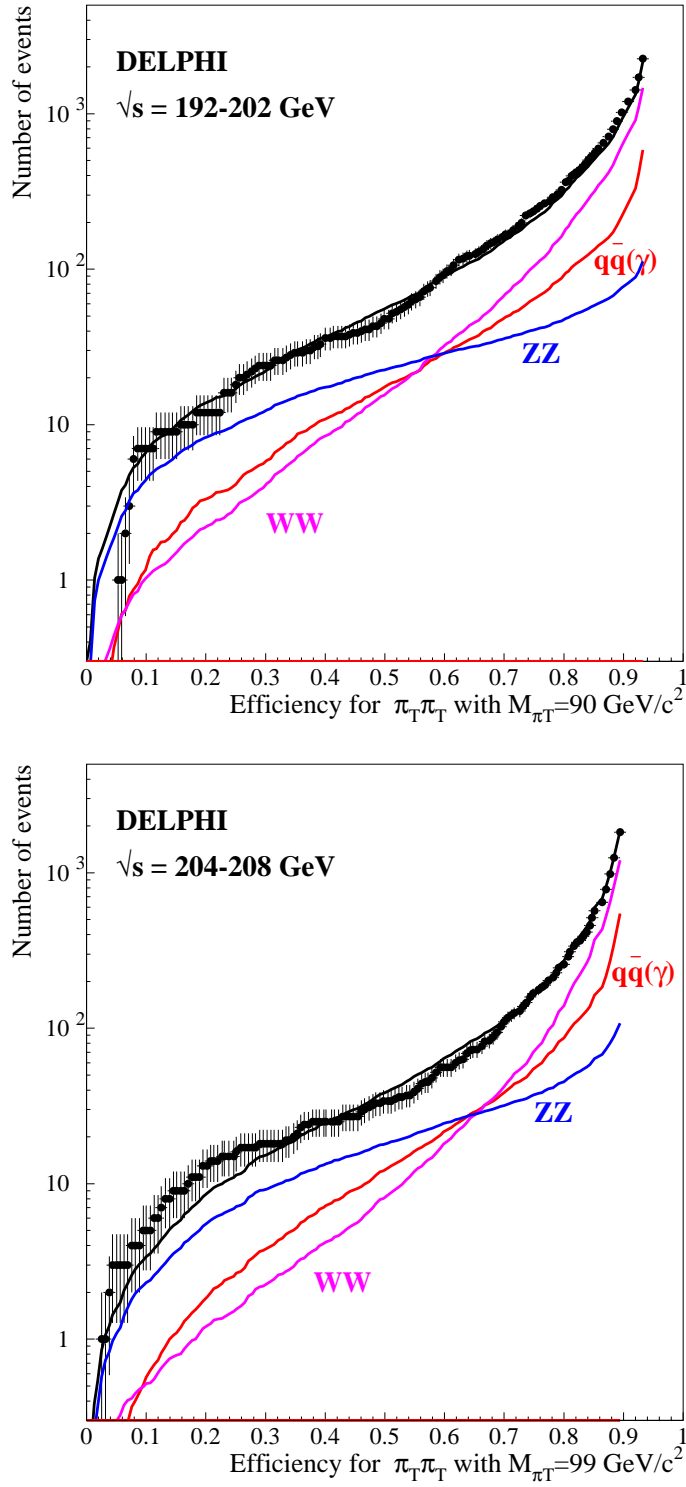


Figure 4: Search in the 4-jet final state: numbers of data events (points) and expected SM background events (curves) as a function of the $\pi_T \pi_T$ signal efficiency, varied by varying the cut on the neural network variable. The different background contributions are shown both separately and combined. The two plots show the two different years of data taking considered.

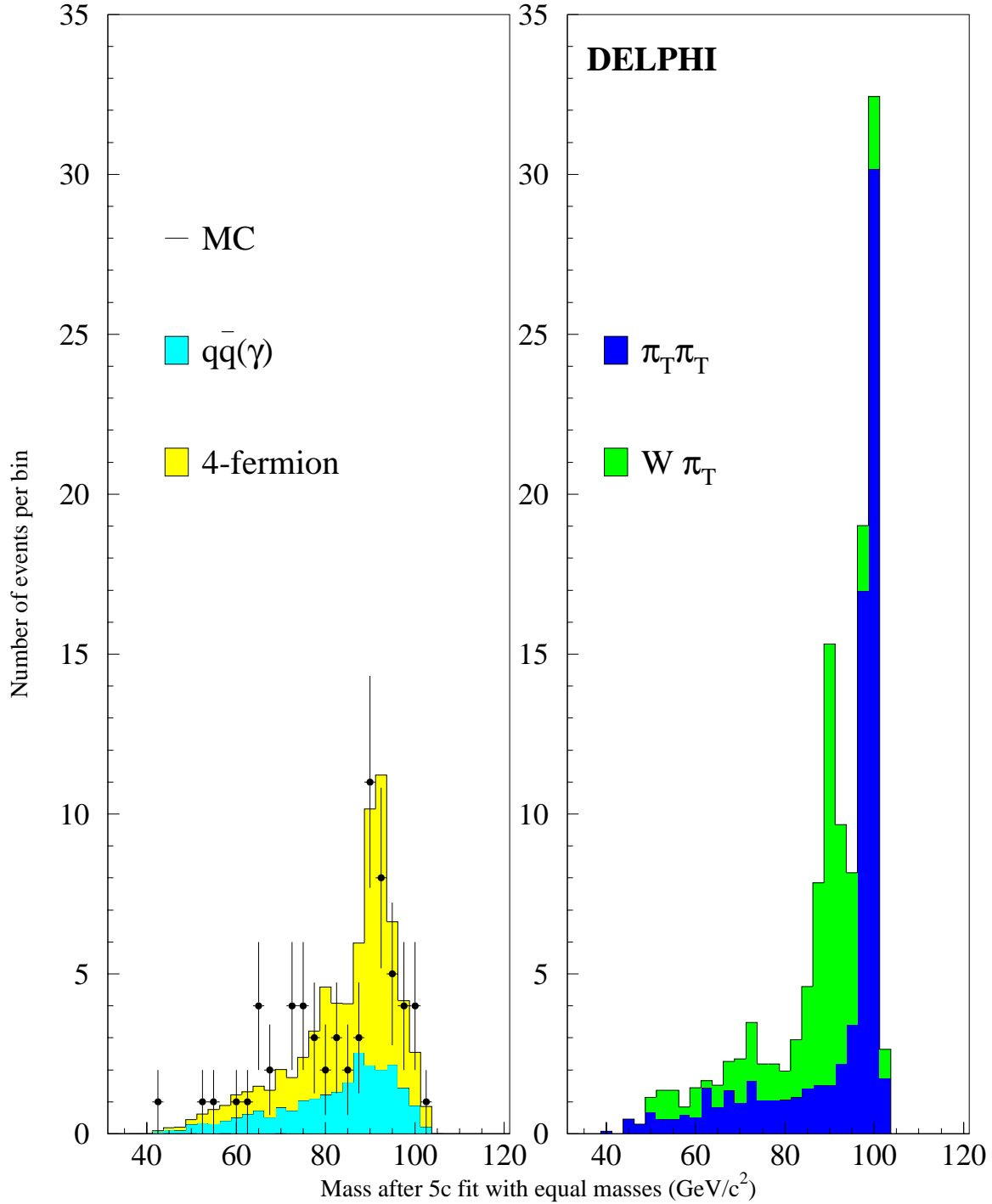


Figure 5: Search in the 4-jet final state: M_{5C} mass distributions for the NN analysis with the cut on NN output > 0.30 . The plot on the left shows the data (points) and the expected SM backgrounds (histograms) for the full DELPHI statistics at $\sqrt{s} = 192 - 208$ GeV. The one on the right shows the technicolor signals in $e^+e^- \rightarrow \pi_T \pi_T$ and $e^+e^- \rightarrow W_L \pi_T$ expected if $M_{\pi_T} = 99$ GeV/c², $M_{\rho_T} = 220$ GeV/c² and $N_D = 9$, normalised to the integrated luminosity collected at $\sqrt{s} = 192 - 208$ GeV.

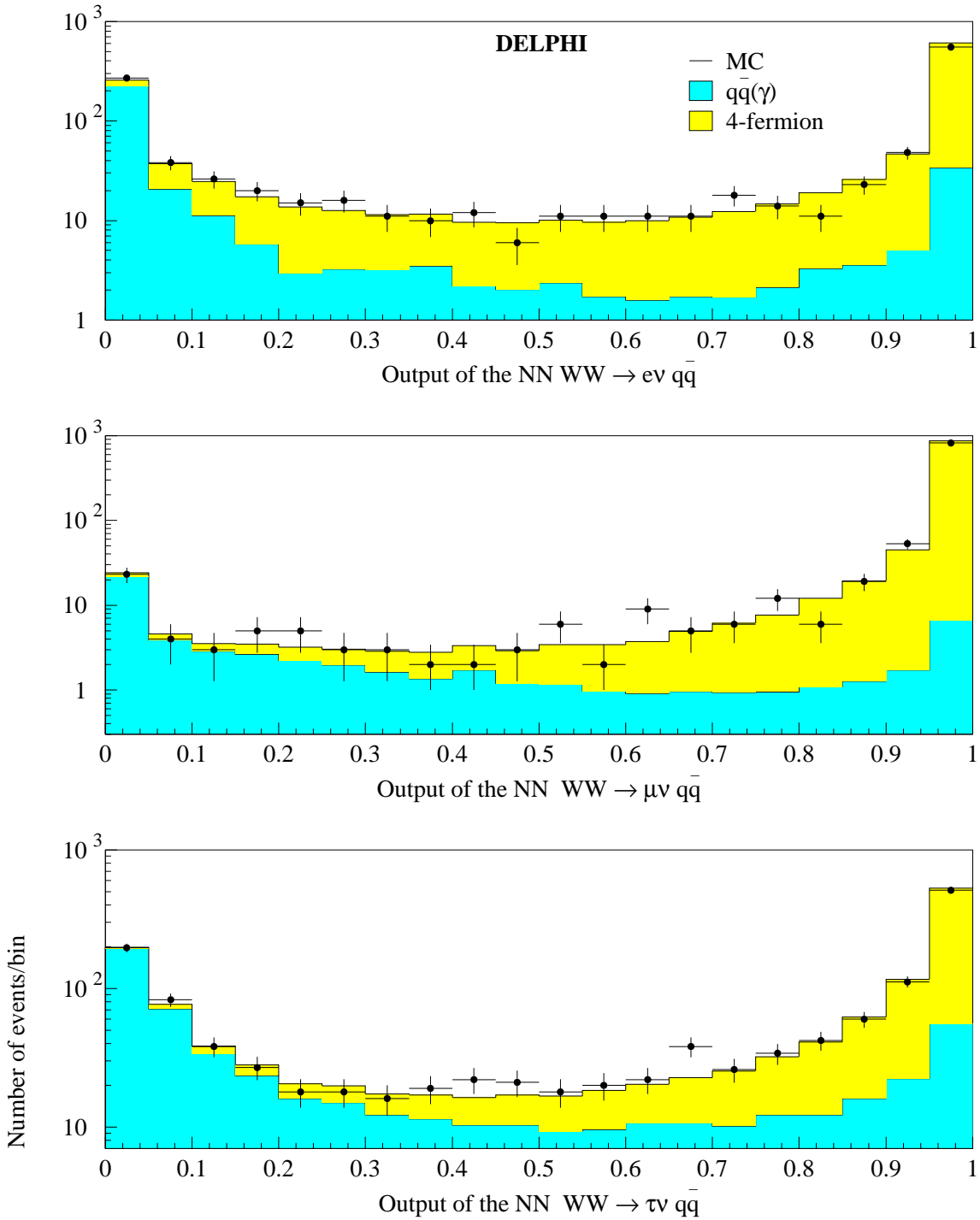


Figure 6: Search in the semileptonic final state: neural network outputs for the rejection of non- WW backgrounds for events with an electron candidate (top), a muon candidate (centre), or a tau candidate (bottom).

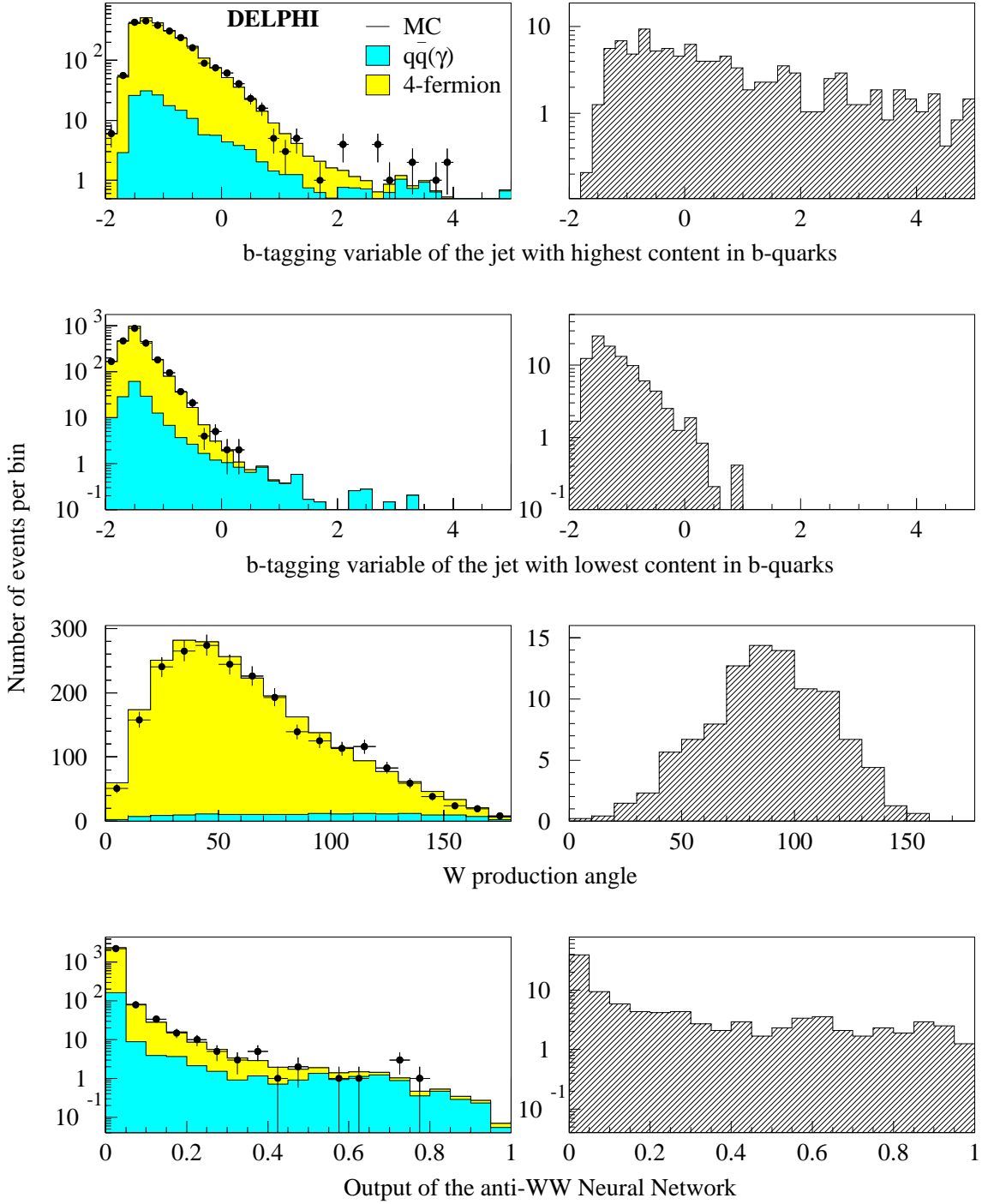


Figure 7: Search in the semileptonic final state: distributions after the rejection of non-WW background. The plots on the left show the data (points) and the expected SM backgrounds (histograms) for the full DELPHI statistics at $\sqrt{s} = 192 - 208$ GeV. Those on the right show the technicolor signal in $e^+e^- \rightarrow W\pi_T$ expected if $M_{\pi_T} = 100$ GeV. The signal normalisation corresponds to $M_{\rho_T} = 220$ GeV/ c^2 , $N_D = 9$ and the integrated luminosity collected at $\sqrt{s}=192-208$ GeV.

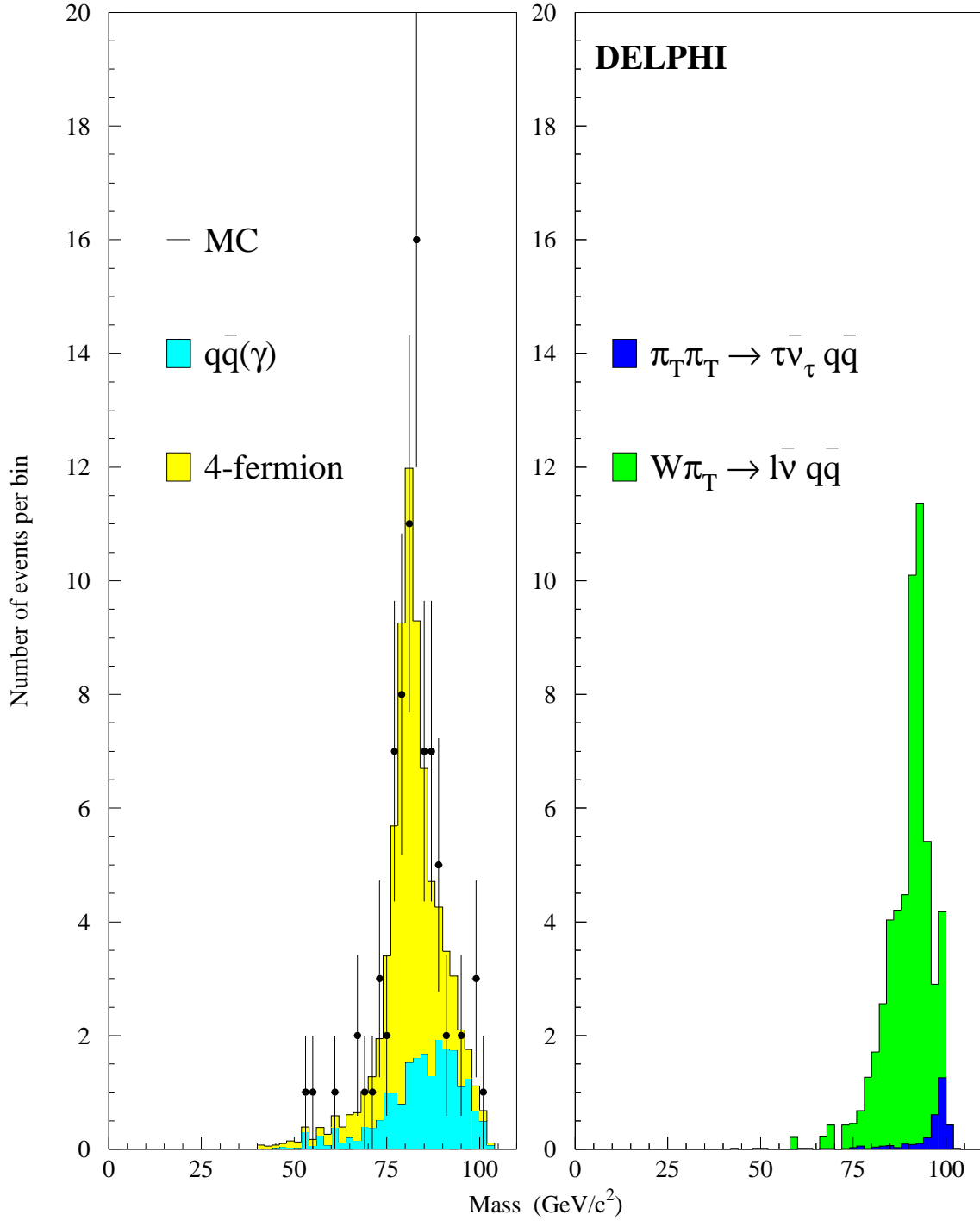


Figure 8: Search in the semileptonic final state: Estimated π_T mass distributions for NN output > 0.10 . The plot on the left shows the data (points) and the expected SM backgrounds (histograms) for the full DELPHI statistics at $\sqrt{s} = 192 - 208$ GeV. The one on the right shows the technicolor signals in $e^+e^- \rightarrow \pi_T \pi_T$ and $e^+e^- \rightarrow W_L \pi_T$ expected if $M_{\pi_T} = 100$ GeV/c², $M_{\rho_T} = 220$ GeV/c² and $N_D = 9$, normalised to the integrated luminosity collected at $\sqrt{s} = 192 - 208$ GeV.

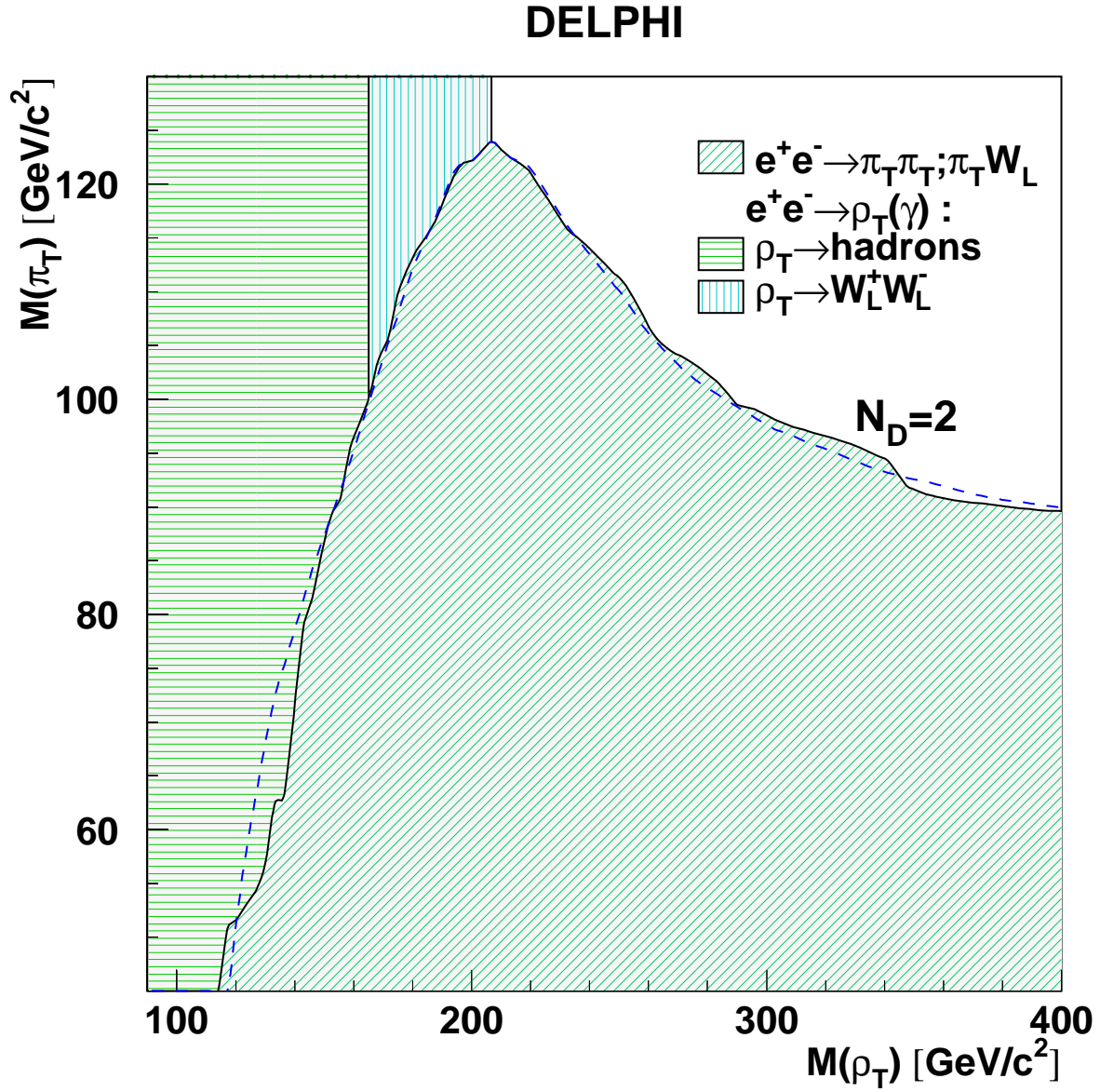


Figure 9: The region in the $(M_{\rho_T} - M_{\pi_T})$ plane (filled area) excluded at 95% CL for $N_D = 2$ (maximal $W_L - \pi_T$ mixing). The dashed line shows the expected limit for the $e^+e^- \rightarrow \pi_T \pi_T, \pi_T W_L$ search.

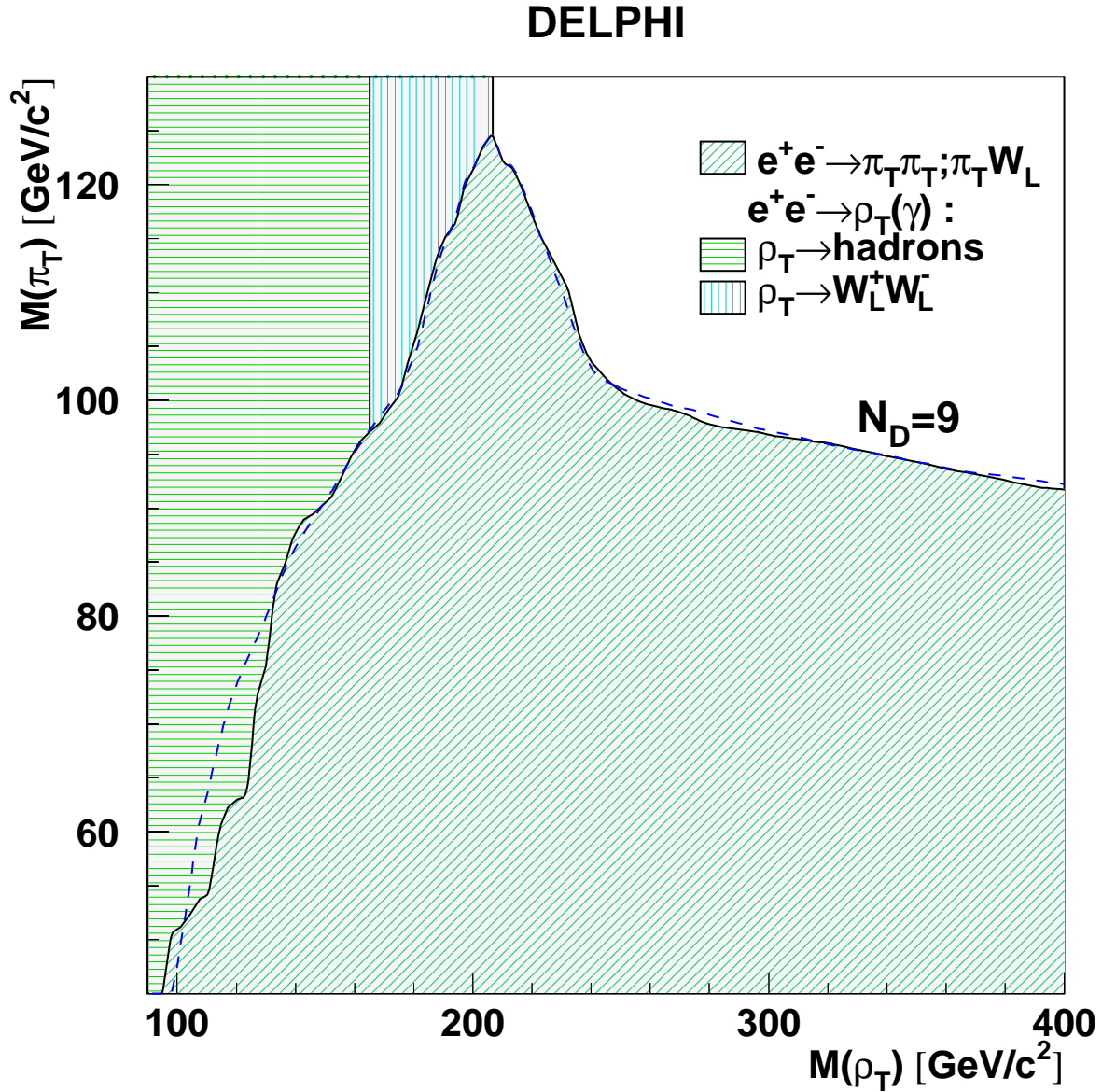


Figure 10: The region in the $(M_{\rho_T} - M_{\pi_T})$ plane (filled area) excluded at 95% CL for $N_D = 9$ (theoretically preferred $W_L - \pi_T$ mixing). The dashed line shows the expected limit for the $e^+e^- \rightarrow \pi_T \pi_T, \pi_T W_L$ search.

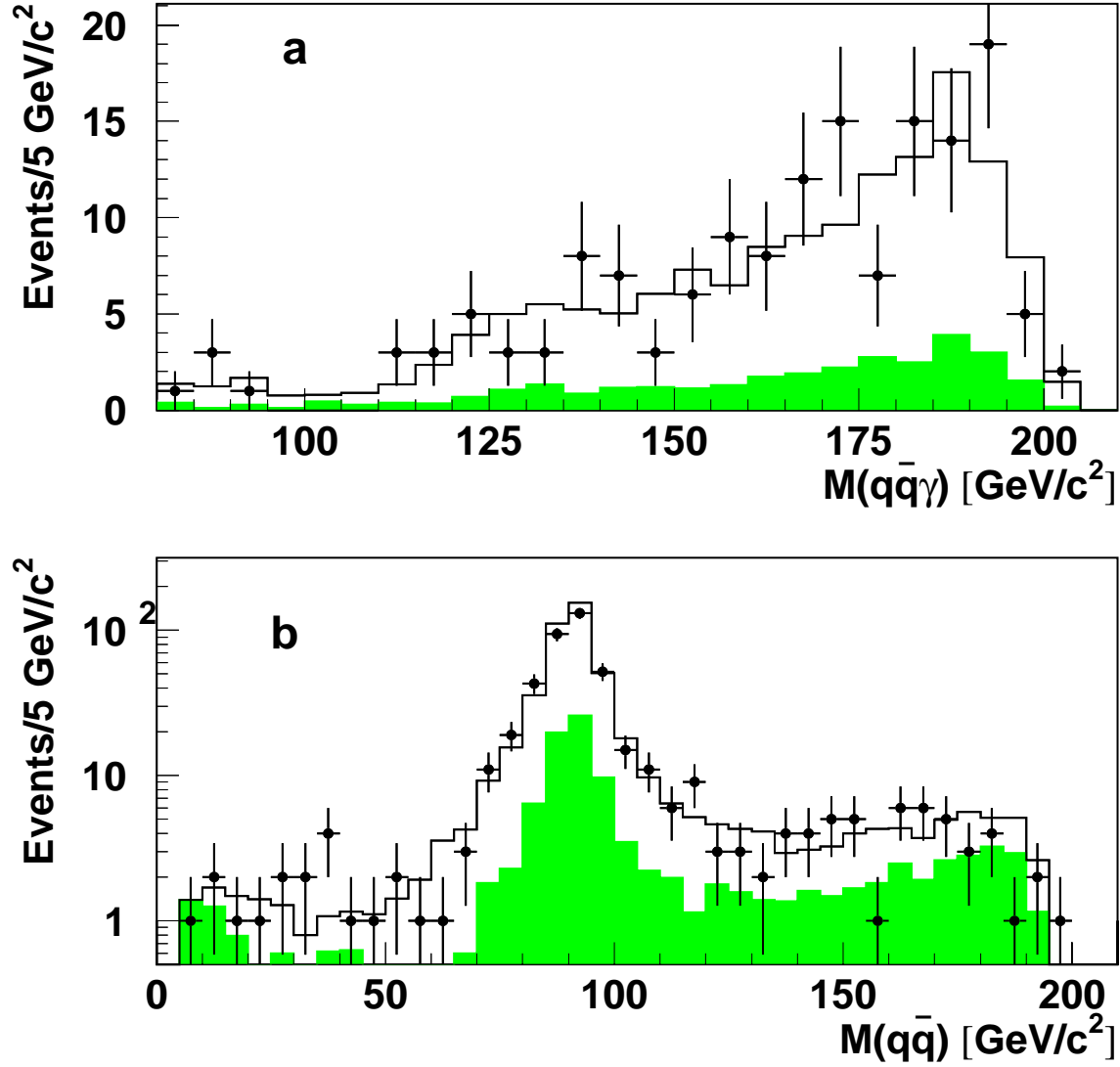


Figure 11: $\pi_T^0\gamma$ analysis: **a)** distribution of the mass of the hadronic system plus the isolated photon; **b)** distribution of the hadronic mass. The points show the data, the histogram shows the contribution of standard sources, and the filled histogram shows separately the contribution of all non- $b\bar{b}\gamma$ processes. The statistics shown in figures **a)** and **b)** corresponds to different event selections, see the text for details.

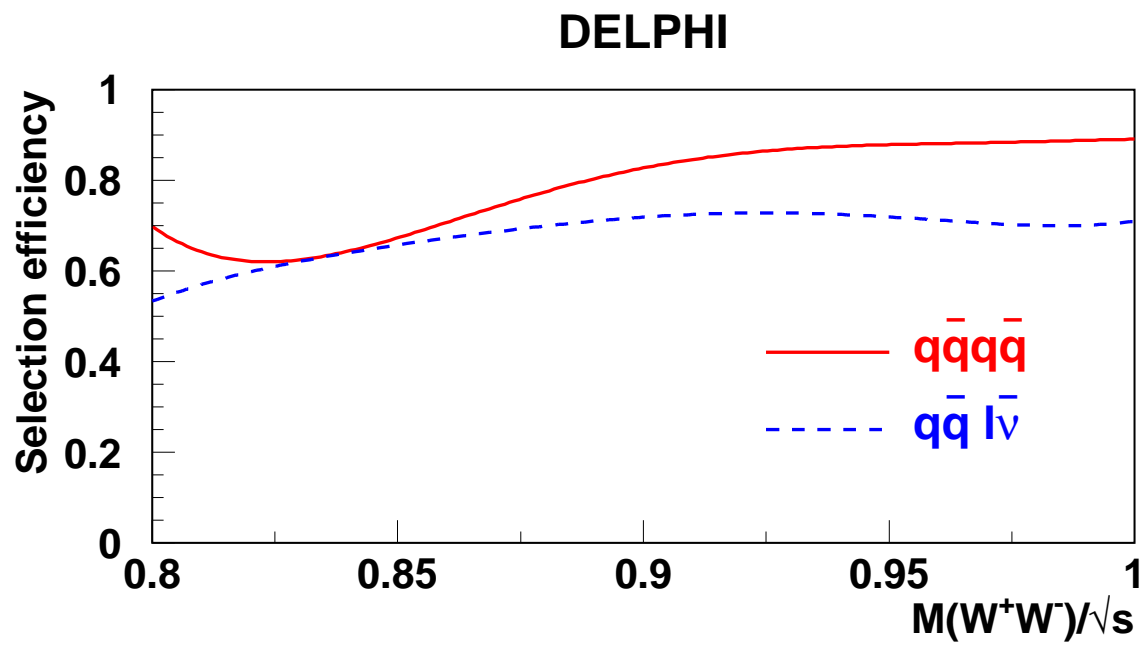


Figure 12: Selection efficiency of a WW -like final state as a function of $M(W^+W^-)/\sqrt{s}$ for $\sqrt{s} = 206$ GeV.

DELPHI

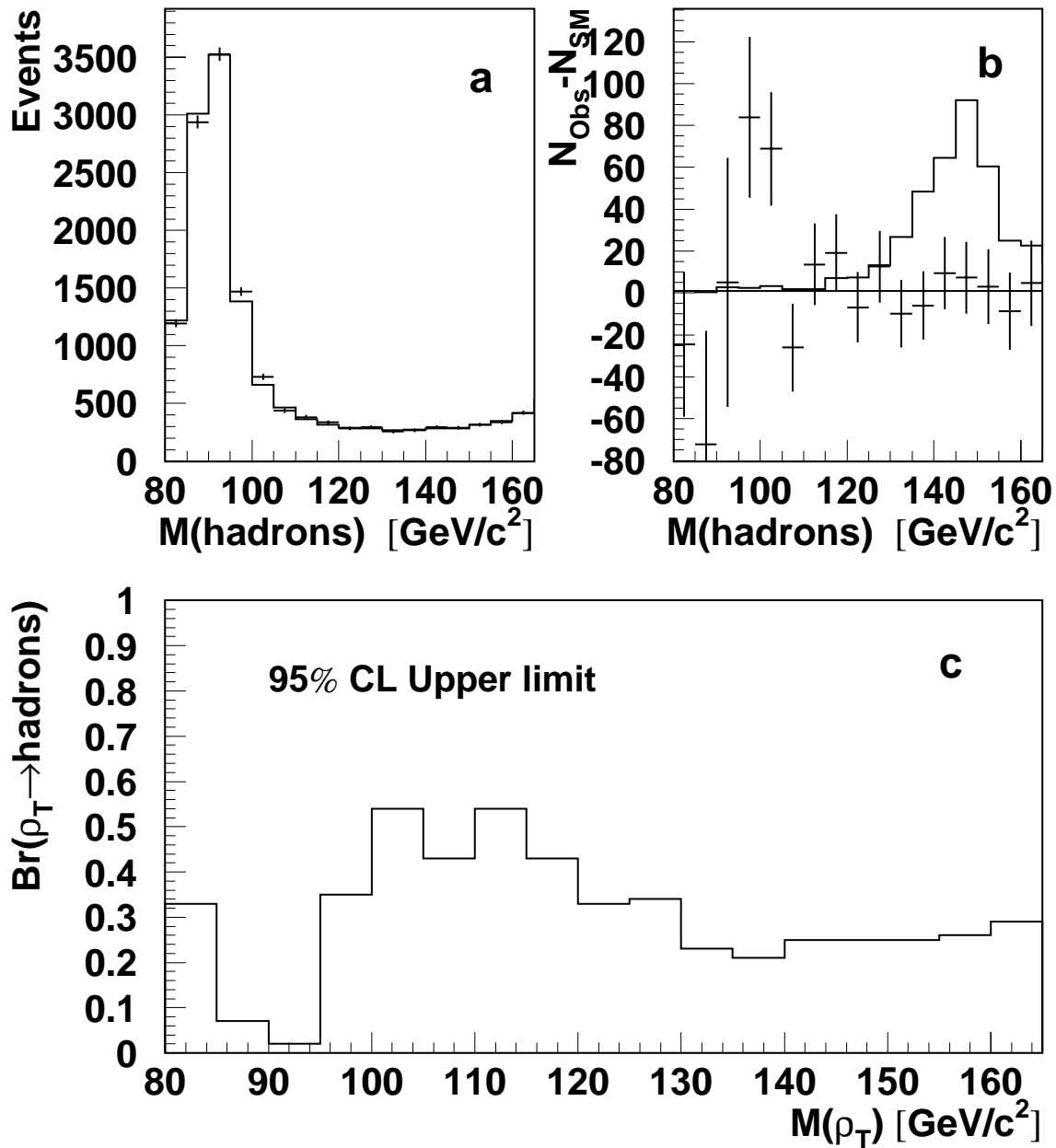


Figure 13: **a)** Mass distribution of the hadronic system in the $e^+e^- \rightarrow q\bar{q}(\gamma)$ analysis for the data collected at $\sqrt{s} = 183$ and 189 GeV . Crosses show the data and the histogram shows the SM contribution. **b)** Difference between the observed numbers of events and those expected in the SM. The expected contribution of $\rho_T \rightarrow \pi_T \pi_T$ with $M_{\rho_T} = 150 \text{ GeV}/c^2$ and $M_{\pi_T} = 70 \text{ GeV}/c^2$ is shown as the histogram. **c)** The 95% CL upper limit on the branching ratio $\text{BR}(\rho_T \rightarrow \text{hadrons})$.

References

- [1] The DELPHI Collab., Nucl. Instr. and Meth. **A303** (1991) 233.
The DELPHI Collab., Nucl. Instr. and Meth. **A378** (1996) 57.
- [2] The DELPHI Collab., Phys. Lett. **B456** (1999) 310.
The DELPHI Collab., Phys. Lett. **B479** (2000) 89.
The LEP Collaborations ALEPH, DELPHI, L3, OPAL, the LEP EW working group and the SLD Heavy Flavour and EW groups, *A Combination of Preliminary Electroweak Measurements and Constraints on the Standard Model*, CERN-EP/2001-021 and e-Print Archive: hep-ex/0103048
P.Buschmann et al. (DELPHI Collab.), *Measurement of the W -pair production cross-section and W branching ratios at $\sqrt{s}=205$ and 207 GeV*, CERN-OPEN/2001-051.
- [3] The DELPHI Collab., Phys. Lett. **B485** (2000) 45.
The DELPHI Collab., Eur.Phys.J. **C11** (1999) 383.
- [4] F.A.Berends, R.Pittau, R.Kleiss, Comp. Phys. Comm. **85** (1995) 437.
- [5] T.Sjöstrand, Comp. Phys. Comm. **39** (1986) 347.
- [6] S. Nova, A. Olshevski and T. Todorov, ‘Physics at LEP2’, CERN 96-01 (1996) Vol.2 p.224; updated version described in ‘Reports of the Working Groups on Precision Calculations for LEP2 Physics’, CERN 2000-009 (2000) 243.
- [7] S.Mrenna, Phys. Lett. **B461** (1999) 352, e-Print Archive: hep-ph/9907201.
- [8] Particle Data Group, in *Review of Particle Physics*, E. Phys. J. **C15** (2000) 103.
- [9] For a recent review see K.Lane, *Technicolor 2000*, preprint BUHEP-00-15 (Boston U.), e-Print Archive: hep-ph/0007304, and references therein.
- [10] See the discussion in T. Barklow et al. *Strong Coupling Electroweak Symmetry Breaking*, preprint SLAC-PUB-7397 (Snowmass 1996), e-Print Archive: hep-ph/9704217 and references therein.
- [11] K.Lane, Phys. Rev. **D60** (1999) 075007, e-Print Archive: hep-ph/9903369;
K.Lane, preprint BUHEP-99-5 (1999), e-Print Archive: hep-ph/9903372.
- [12] The CDF Collab., Phys. Rev. Lett. **83** (1999) 3124.
The CDF Collab., Phys. Rev. Lett. **84** (2000) 1110.
- [13] S.Catani, Yu.L.Dokshitzer, M.Olsson, G.Turnock, B.R.Webber, Phys. Lett. **B269** (1991) 432.
- [14] The DELPHI Collab., Phys. Lett. **B499** (2001) 23.
- [15] The DELPHI Collab., P.Abreu et al., Eur. Phys. J. **C10** (1999) 563.
- [16] G.Borisov, Nucl. Instr. Meth. **A417** (1998) 384.
The DELPHI Collab., Eur. Phys. J. **C10** (1999) 415.
- [17] P.Abreu et al, Nucl. Instr. and Meth. **A427** (1999) 487.
- [18] A.L. Read, *Modified Frequentist Analysis of Search Results (The CL_s method)*, 1st Workshop on Confidence Limits, CERN, Geneva, Switzerland, CERN Report 2000-005, p. 81 (2000).
- [19] The L3 Collab., Phys. Lett. **B496** (2000) 34.
- [20] ALEPH, DELPHI, L3 and OPAL Collaborations, *Searches for Higgs bosons: Preliminary combined results using LEP data collected at energies up to 202 GeV*, preprint CERN-EP/2000-055 (2000).
- [21] A.Denner et al., Phys. Lett. **B475** (2000) 127.